Journal of Catalysis 414 (2022) 163–178

Contents lists available at ScienceDirect

Journal of Catalysis

journal homepage: www.elsevier.com/locate/jcat

Selective production of imines and benzimidazoles by cooperative bismuth(III)/transition metal ion catalysis

Marianna Kocsis [a,b], Márton Szabados [a,b], Sándor B. Ötvös [c,*], Gergely F. Samu [d,e], Zsolt Fogarassy [f], Béla Pécz [f], Ákos Kukovecz [g], Zoltán Kónya [g,h], Pál Sipos [b,i], István Pálinkó [a,b,1], Gábor Varga [b,j,*]

[a] Department of Organic Chemistry, University of Szeged, Dóm tér 8, Szeged H-6720, Hungary
[b] Materials and Solution Structure Research Group, and Interdisciplinary Excellence Centre, Institute of Chemistry, University of Szeged, Aradi Vértanúk tere 1, Szeged H-6720, Hungary
[c] Institute of Chemistry, University of Graz, NAWI Graz, Heinrichstrasse 28, Graz A-8010, Austria
[d] Department of Physical Chemistry and Materials Science, Interdisciplinary Excellence Centre, University of Szeged, Szeged H-6720, Hungary
[e] ELI-ALPS Research Institute, Szeged H-6728, Hungary
[f] Institute of Technical Physics and Materials Sciences, Centre for Energy Research, H.A.S., H-1121 Budapest, Konkoly Thege M. út 29-33, Hungary
[g] Department of Applied and Environmental Chemistry, University of Szeged, Rerrich Béla tér 1, Szeged H-6720, Hungary
[h] MTA-SZTE Reaction Kinetics and Surface Chemistry Research Group, Rerrich Béla tér 1, Szeged H-6720, Hungary
[i] Department of Inorganic and Analytical Chemistry, University of Szeged, Dóm tér 7, Szeged H-6720, Hungary
[j] Department of Physical Chemistry and Materials Science, University of Szeged, Rerrich Béla tér 1, Szeged H-6720, Hungary

ARTICLE INFO

Article history:
Received 25 July 2022
Revised 7 September 2022
Accepted 8 September 2022
Available online 14 September 2022

Keywords:
Oxidative annulations
Lewis acid co-catalysts
Synergetic Lewis acid/Mn(II) or Co(II) heterogeneous catalysis
Water-tolerance syntheses of benzimidazoles

ABSTRACT

Cooperative Bi(III)/Co(II) and Bi(III)/Mn(II) heterogeneous catalysts have been developed enabling efficient oxidative annulations for preparing both cross-coupled imines and benzimidazoles under ambient conditions in an atom-economic and time-efficient manner, involving ambient air as oxidant and without the need of any other additives. This is the first synergistic Lewis acid/transition metal catalyzed annulation which is potentiated by the interfaces between the building blocks of the catalysts. To achieve our goals, a useful fabrication process has been developed to heterogenize the transition metal ions *via* strong interactions on well-known Sillèn-type bismuth subcarbonate (bismutite). Their reusability, activity and selectivity as well as water-tolerance have made them potential competitors to effective heterogeneous/homogeneous catalysts reported previously.

1. Introduction

Because of their diverse applications, much attention have been paid to nitrogen-containing heterocyclic compounds and their syntheses for many years [1]. Prominent reactions among these are the oxidative cross couplings and oxidative annulations of anilines and amines, being key processes, both in industry and in academia to produce fine chemicals such as pharmaceuticals [2,3], functional materials [4–7] or chemical sensors [8,9]. For annulations, the most efficient catalysts are typically based on Brønsted and Lewis acids such as *N*-hydroxyphthalimide [10], $In(OTf)_3$ [11] or $VO(acac)_2$–$CeCl_3$ [12] *etc.*, including both homogeneous and heterogeneous ones yielding benzimidazole products selectively. In fact, extension of the scope of application to some well-known, promising Lewis acids such as Sn- [13] and Bi-compounds [14] as of yet did not occur. More recently, both photoinduced noble metal catalysis as well as metal-free homogeneous processes have been successfully introduced [10,15–18]. However, because of the extreme likelihood of their homocoupling, instead of the amines, (aromatic) alcohols as reaction partners with anilines have been applied more frequently (Table S1). Oxidative cross couplings of anilines and amines toward imines could be catalyzed by using noble metals or non-metallic specimens as promoters (Table S1) [16,19–26]. It has become also evident that catalytic imine and benzimidazole syntheses can readily be performed by applying 3d transition metal ions as promoters [27–32]. Nevertheless, the widespread use of these valuable metals as catalysts in these annulations/couplings are hindered by the fact that non-commercial oxidation state of the metal ions must be stabilized to ensure catalytic efficacy [33]. Additionally, organic/inorganic additives are typically required due to their well-known impact on the charge value of the metal ions and on intermediates of the reactions [34].

* Corresponding authors at: Department of Physical Chemistry and Materials Science, University of Szeged, Rerrich Béla tér 1, Szeged H-6720, Hungary (G. Varga).
E-mail addresses: sandor.oetvoes@uni-graz.at (S.B. Ötvös), gabor.varga5@chem.u-szeged.hu (G. Varga).
[1] Passed away.

https://doi.org/10.1016/j.jcat.2022.09.008
0021-9517/

Importantly, most of the known catalytic reactions are homogeneous processes. For example, commercial Co(II),[35] Fe(II)[36]/Fe(III)[35,37] and Cu(I)[38]/Cu(II) [2,39] salts have also proven to be efficient, however, recycling a reuse of these materials would be highly cumbersome. Furthermore, in numerous examples, due to the self-coupling of the reactants, high amounts of by-products were generated *via* unwanted catalytic processes. Despite the clear limitations of these strategies in reaction time (24–72 h), reaction temperature (120–150 °C), as well as the lack of recyclability, low selectivity and the high price of the catalysts, these Lewis acids and transition metal ions are still widely used. Although, in most of these reactions O_2 was used as a green oxidant, using ambient air is more practical, less expensive and safer [40,41]. Additionally, the development of water-tolerant reactions and annulations in green media have also remained a synthetic challenge. The utilization of high performance manganese- and nickel-based catalysts, which are known to bear great promises as catalysts in green chemical approaches [42], is still largely underexplored. To the best of our knowledge, only some aspects of manganese promoted cyclocondensations have been investigated so far [43].

In order to successfully address these challenges, cooperative catalysis with the aid of Lewis acids and (3d) transition metal ions with variable charge could provide an interesting new perspective [44–47]. 3d transition metal ions with cooperation of main group Lewis acids and/or non-metallic components have already been found efficient for enabling, among others, C–H activation and C–N bond formation reactions [48,49]. Surprisingly, in oxidative annulations, bismuth-based cooperative catalysts are less widely known, despite their useful features in bismuth-mediated reactions for tandem-like reactions [14,50]. Generally, Lewis acid centers as co-catalysts generate intermediates, forming coordinative bonds with the reactant(s), to ease the insertion of the "main" catalyst. By using cooperative catalysts, cost effective, atom economic as well as reasonably fast catalytic reactions are possible. Contrary to their meaningful catalytic features, cooperative catalytic oxidative reactions currently bear strong limitations in terms of catalyst recycling and reuse [51]. To ensure the optimal operation of the cooperative catalysts, such reactions are typically performed as homogeneous catalytic processes.

These limitations inspired us to design and develop Lewis acid/3d transition metal ion cooperative catalysts with tuneable catalytic ability to promote both oxidative coupling and annulation of o-phenylenediamine (2-aminoaniline) with benzylamine and its derivatives under mild reaction conditions. The envisioned way of catalysis would provide an option to control reaction pathways, thus isolating imines (coupling product) or benzimidazoles (annulation product) selectively (depending on the reaction parameters) without the undesired self-coupling of benzylamine. Considering that we successfully presented previously that transition metal-inserted Sillèn-type bismuth-containing species (bismutites) can operate as heterogeneous cooperative catalysts toward concerted heterocyclizations and couplings [52–56], the main goal herein was to achieve heterogeneous cooperative catalysis by applying non-commercial bismuth-based specimens, especially bismutites, as Lewis acid sites. To the best of our knowledge, no data can be found in the literature about the catalytic application of similar heterogeneous catalysts in oxidative annulations.

Herein, by using Sillèn-type bismutite structure and transition metal species (Co(II), Mn(II), Ni(II)) as building blocks, the construction of cooperative catalytic composite systems *via* different synthesis strategies is reported (Scheme 1). The as prepared catalysts were used to promote oxidative transformations of *o*-phenylenediamine and its isosteres with amines to form imines or benzimidazoles in a highly tuneable manner. To produce strongly bonded metal species, a modified co-precipitation strategy was employed while grafting of potentially active centres *via* weak interaction was fixed by wet impregnation (Scheme 1). The most important findings presented here include (i) proof of catalytic ability of bismuth-based Lewis acid catalysts for oxidative cross coupling and annulation of amines; (ii) effective synthesis of well-characterised surface modified Sillèn-type structures; (iii) first cooperative Lewis acid/transition metal catalysed C–H/N–H annulations; (iv) water-tolerant, recyclable and effective heterogeneous catalytic processes for forming both 2-(benzylideneamino) aniline and benzimidazoles and its structural isosteres under mild reaction conditions and (v) the demonstration of the effect of the interface between the building blocks on the catalytic efficiency.

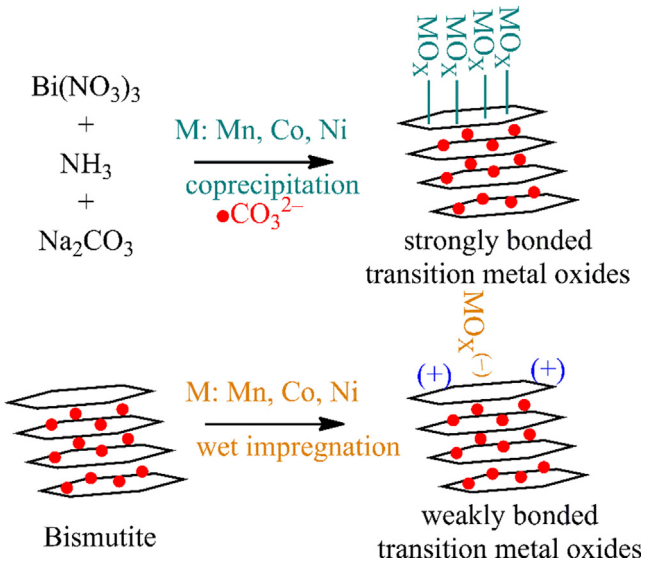

Scheme 1. Foreseen synthesis strategies for producing bismutite-supported transition metal oxide (cooperative) catalysts.

2. Experimental section

2.1. General information

Manganese(II) oxide (99%, MnO), manganese(II) nitrate hexahydrate (98%, $Mn(NO_3)_2{\cdot}6H_2O$), manganese(II,III(IV)) oxide (99%, Mn_3O_4), manganese(III) oxide (99%, Mn_2O_3), manganese(IV) oxide (99%, MnO_2), cobalt(II) oxide (99%, CoO), cobalt(II) hydroxide (98%, $Co(OH)_2$), cobalt(II) nitrate hexahydrate (99%, $Co(NO_3)_2{\cdot}6H_2O$), cobalt(II,III) oxide (99%, Co_3O_4), nickel(II) oxide (99%, NiO), nickel(II) hydroxide (98%, $Ni(OH)_2$), nickel(II) nitrate hexahydrate (98%, $Ni(NO_3)_2{\cdot}6H_2O$), nickel(III) oxide hydroxide (98%, NiOOH), bismuth(III) oxide (98%, Bi_2O_3), bismuth(III) nitrate pentahydrate (98%, $Bi(NO_3)_3{\cdot}5H_2O$), bismuth(III) iodide (97%, BiI_3), bismuth(III) chloride (97%, $BiCl_3$), Bi(III) oxychloride (96%, BiOCl), sodium bismuth(V) oxide (95%, $NaBiO_3$; sodium bismuthate), ammonia solution (25%, NH_4OH); sodium carbonate (99%, Na_2CO_3), sodium bicarbonate (99%, $NaHCO_3$), concentrated nitric acid (99%, cc. HNO_3), sodium sulphate anhydrous (98%, Na_2SO_4), sodium chloride (98%, NaCl), dimethyl sulfoxide (99%, C_2H_6OS; DMSO), 5-methyloxolan-2-one (99%, $C_5H_8O_2$; γ-valerolactone), *N*,*N*-dimethylformamide (99%, $HCON(CH_3)_2$; DMF), toluene (97%, $C_6H_5CH_3$), ethyl acetate (98%, $CH_3COOCH_2CH_3$; EtOAc), hexane (99%, C_6H_{14}), acetonitrile (98%, C_2H_3N; MeCN), benzylamine (99%, $C_6H_5CH_2NH_2$), 2-aminoaniline (99%, $C_6H_4(NH_2)_2$; *o*-phenylenediamine), 2-aminophenol (99%, $C_6H_4NH_2OH$), 2-aminothiophenol (99%, $C_6H_4NH_2SH$), 4-methoxybenzylamine (98%, $CH_3OC_6H_4CH_2NH_2$), 2-methoxybenzylamine (98%, $C_6H_4CH_2NH_2OCH_3$), 4-chlorobenzylamine (99%, $ClC_6H_4CH_2NH_2$),

2-chlorobenzylamine (97%, $C_6H_4CH_2NH_2Cl$), 3-nitrobenzylamine hydrochloride (98%, $O_2NC_6H_4CH_2NH_2 \times HCl$), aniline (99.5%, $C_6H_5NH_2$), ethanol (96%, C_6H_5OH), deuterated dimethyl sulfoxide (99.9%, C_2D_6OS; DMSO d_6) were purchased from commercial sources and used as received. Purified water was produced by reverse osmosis and UV irradiation processes by a Puranity TU 3 + UV/UF system (VWR).

2.2. Synthesis of transition metal-containing bismutites via modified co-precipitation method

To prepare bismutite-based composite catalysts with strongly bonded transition metal specimens, a modified co-precipitation method was applied. The appropriate amounts of $Bi(NO_3)_3{\cdot}5H_2O$ (3.75 mmol) in the presence of the corresponding transition metal salts (3.75 mmol) were dissolved in 25 mL of 5 wt% aqueous citric acid solution. After that, 40–40 mL of 0.4–0.4 M ammonia and sodium carbonate solutions were added dropwise into the metal salt solution, and was stirred at 100 °C for 24 h. The obtained crude product was filtered, washed with distilled water and ethanol several times, and dried at 60 °C overnight. The solidified product was marked as $MBi_2O_2CO_3$ (M: Ni, Co or Mn) (designated as co-precipitated samples). For comparison, transition metal-free bismutite ($Bi_2O_2CO_3$) was also obtained in the same way without loading the corresponding transition metal salt.

2.3. Preparation of bismuth subcarbonate-supported NiO_x, MnO_x and CoO_x

For the preparation of bismuth subcarbonate-supported NiO_x/MnO_x/CoO_x catalysts, a wet impregnation method was employed. First, colloidal suspensions of transition metal salts (5 mg/mL) were prepared in ethanol. The desired amounts of solution (transition metal salt of 5–15 wt%) were added to one portion of the bismuth subcarbonate (0.5 g), and the mixtures were sonicated for 2 h at room temperature. The obtained dark intermediates were separated by filtration, thoroughly washed with ethanol and water several times, and dried in an oven at 60 °C overnight. These solids were then heat-treated at 250 °C for 8 h to obtain the products. The as-prepared bismutite-supported transition metal-containing catalyst were labelled as $M{-}Bi_2O_2CO_3$ (M: Ni, Co or Mn) (designated as impregnated samples).

2.4. Characterization methods

X-ray diffraction (XRD) patterns were detected with a Rigaku XRD-MiniFlex II instrument using CuK_α radiation (λ = 0.15418 n m) and 40 kV accelerating voltage at 30 mA. The characteristic reflections in the normalized diffractograms were identified on the basis of JCPDS-ICDD (Joint Committee of Powder Diffraction Standards- International Centre for Diffraction Data) database.

Thermogravimetric analyses were performed on a Setaram Labsys derivatograph. Samples were heated at a rate of 1 °C min^{-1} to 600 °C under an air flow. The samples of 30–35 mg were put into high-purity alpha alumina crucibles. For carrying out evolved gas analysis (EGA), a Pfeiffer QMS 200 mass spectrometer was applied under an air flow (40 mL/min) with 5 °C/min heating rate preparing ~ 100 mg samples for each them.

The structure-building inorganic components were identified by (FT-)IR and (FT-)Raman spectroscopies. Using an IR source of 785 nm wavelength, Raman spectra of 4 cm^{-1} resolution were taken by a Raman Senterra II (Bruker) microscope using a laser intensity of 12.5 mW, 50-fold objective magnification of and an integration time of 50 s. The mid infrared (IR) spectra of the composites were detected in the spectral range of 4000–600 cm^{-1} by using a BIO-RAD FTS-65A/896 spectrometer. Spectral resolution was 4 cm^{-1} and 256 scans were applied for each spectrum in attenuated total reflection (ATR) detection mode for which a Harrick's single reflection diamond ATR accessory was used.

The first coordination sphere and oxidation state of the transition metal ions was established by using a combined UV–Vis spectrophotometric - X-ray photoelectron (XP) spectroscopic mapping. UV–Vis spectra were taken by a SHIMADZU UV-3600i Plus UV–Vis-NIR spectrophotometer equipped with PMT, InGaAs and PbS detectors, in the 50000–6000 cm^{-1} wavenumber range with 4 cm^{-1} resolution. Measurements were performed in the reflection mode. X-ray photoelectron spectra (XPS) were recorded with a SPECS instrument equipped with a PHOIBOS 150 MCD 9 hemispherical analyzer, under a main-chamber pressure in the 10^{-9}–10^{-10} mbar range. The analyzer was run in the fixed analyzer transmission (FAT) mode with 20 eV pass energy. The Al K_α radiation ($h\nu$ = 14 86.6 eV) of a dual anode X-ray gun was applied as an excitation source. The gun was operated at 210 W power (14 kV, 15 mA). The binding energy scale was corrected by setting the main C 1 s component to 285.0 eV in all cases, corresponding to the adventitious carbon. For spectrum acquisition and evaluation, commercial (CasaXPS, Origin) software packages were used.

The elemental imaging of the freshly prepared samples was studied by scanning electron microscopy coupled to energy dispersive X-ray spectrometer (SEM-EDX). The SEM images were registered on an S-4700 scanning electron microscope (SEM, Hitachi, Japan) with an accelerating voltage of 10–18 kV. EDX data were obtained with a Röntec QX2 energy dispersive microanalytical system. The coupled system also provided with the elemental map. High-resolution, HAADF (high-angle annular dark-field) TEM imaging was carried out utilizing a JEOL 2100F TEM (field emission gun source, information limit < 0.19 nm) at 100 kV at room temperature. (TEM-)EDX spectra were taken by applying an Oxford Instruments 30 mm^2 Si(Li)detector or an Oxford Instruments x-Max 80 SDD running on an INCA microanalysis system. To prepare samples for TEM(–EDX) measurements, several drips of a suspension of each composite was dropped onto copper-grid mounted "lacey" carbon films.

The metal ion ratio of the as-prepared composites and the possible leaching during the catalytic processes was measured by ICP–MS on an Agilent 7700x instrument. Before measurements, few micrograms of the samples measured by analytical accuracy were dissolved in 1 mL concentrated nitric acid, followed by dilution with distilled water to 50 mL and filtration.

2.5. General procedure for oxidative coupling/annulation

To a solution of 2-aminoaniline (*o*-phenylenediamine; 2.0 mmol; **(2)**) and benzylamine (2.4 mmol; **(1)**) in an appropriate solvent or solvent mixture (2 mL), a selected catalyst composite was added (corresponding to at least 2.5 mol% that is 4×10^{-3} - mmol metal ion loading), and the slurry was stirred at $\leq$ 70 °C for the appropriate time under ambient air atmosphere. The progress of the reaction was monitored by thin layer chromatography (TLC) using mixtures of ethyl acetate and hexane as eluent. The obtained mixture was cooled to room temperature and treated with saturated $NaHCO^3$ (5 mL) followed by extraction with ethyl acetate (3×10 mL) and washing with brine (2×5 mL) and water (1×5 mL). The conversion and selectivity were determined after each reaction by ^1H NMR using a 500 MHz Bruker DRX500 instrument and DMSO d_6 as solvent at room temperature. In some cases, for comparison, the above test reaction was repeated under the optimized reaction conditions without the addition of 2-aminoaniline to test the catalytic ability of the building blocks of the composite catalysts.

In reaction of benzylamine **(1)** and 2-aminoaniline **(2)** (Scheme 2), 2-(benzylideneamino)aniline (also mentioned as

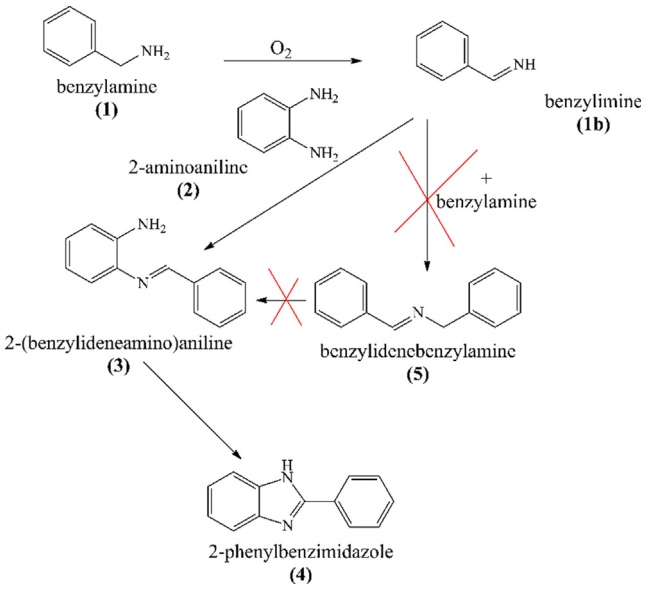

Scheme 2. Oxidative coupling of benzylamine and 2-aminoaniline involving ambient air as oxidant.

oxidative coupling product; **(3)**) and/or 2-phenylbenzimidazole (oxidative annulation product; **(4)**) were obtained as main products. The selectivity of the process was fine-tuned with the reaction conditions. The aim of the optimization procedure was to maximize these yields without producing benzylidenebenzylamine (self-coupling product of benzylamine; **(5)**) by-product.

After the oxidative transformations, the active catalyst was separated from the reaction mixture by centrifugation followed by thorough washing with ethanol, water and DMSO. The catalyst samples were reutilized in the following runs under the optimized reaction conditions. In each run, the filtrate was checked by ICP-MS to detect any leaching of the metallic components of the catalysts. To determine the structural integrity of the composites after each run, *ex situ* XRD study on the used catalysts was performed. To ascertain the heterogeneous nature of the reactions, the hot filtration test was carried out as follows. The catalytic composite was filtrated from the reaction slurry before completion of the transformation (around 50% benzylamine conversion) and then the filtrate was further treated under unchanged reaction conditions.

3. Results and discussion

3.1. Bismuth compound and solvent screening for catalytic conversion of benzylamine

First, some commercial and self-prepared bismuth compounds were tested in the oxidative reaction of *o*-phenylenediamine (2-aminoaniline; **(2)**) with benzylamine **(1)**. In comparison with the reaction parameters reported previously (Table S1), milder reaction conditions were chosen for the initial set (10 mol% Bi, DMSO, 24 h at 110 °C). As shown in Table 1, commercial bismuth salts proved ineffective as catalysts for the oxidative transformations with conversions (~4%) comparable to that of the uncatalyzed reaction. This finding is in line with the observations published previously [12]. On the contrary, both Bi_2O_3 (11% conversion) and $Bi_2O_2CO_3$ (bismutite; 19% conversion) showed moderate activity in this reaction, resulting in a slight improvement in benzylamine conversion. Note that a heat treatment at ~ 150 °C was necessary to remove surface adsorbed water and thus to activate bismutite to reach the observed catalytic efficiency. It should also be noted that the active promoters showed selectivity of ~ 80% toward the undesired self-coupling product **(5)** of benzylamine. Importantly, both the selectivity and the reaction rate of both oxidative transformations are generally affected by the solvents used. Thus, in addition to DMSO, other environmentally acceptable solvents were tested (Fig. 1). No reaction was detected in water, 2-MeTHF and under solvent-free conditions, while significant changes in both conversion and selectivity were observed in DMSO:water mixtures and also in γ-valerolactone. As a result of the solvent exchange, besides enhanced benzylamine conversion, notable increase in product selectivity occurred. The rate of benzylamine self-coupling **(5)** gradually decreased with rising water-content in DMSO, until it totally disappeared upon using a DMSO:H_2O mixture of 1:9. γ-Valerolactone as solvent was also found useful in minimizing side reactions. Not only did these solvents drive back the self-coupling side reaction, but they also improved the selectivity towards the oxidative coupling **(3)** and oxidative annulation products **(4)**. To summarize, benzylamine conversion in different solvents decreased according to the following trends over both active catalysts: DMSO:H_2O 1:9 > DMSO:H_2O 1:1 > DMSO:H_2O 9:1 > γ-valer olactone > DMSO. A similar trend was found in the increase of the selectivity of the desired products, however, γ-valerolactone was not fitting in this series. It became evident from the bismuth compound screening that bismuth-based catalysts possess valuable catalytic activity for such reactions, approximating the catalytic ability of the most frequently used homogeneous catalysts. Moreover, $Bi_2O_2CO_3$ as versatile Lewis acidic building block seemed to be a right option for the development of an efficient cooperative catalyst. Using $Bi_2O_2CO_3$ as catalyst in DMSO:H_2O 1:9, a benzylamine conversion of 69% with 2-phenylbenzimidazole **(4)** selectivity of 73% was obtained; these values were considered as benchmark values for the further optimization procedures.

As prospective building blocks for cooperative catalysts, pure 3d transition metal oxides were also tested in oxidative coupling of benzylamine **(1)** and 2-aminoaniline **(2)** under similar reaction conditions as shown above (Table 2). It was observed that only MnO_2, Mn_3O_4 and Co_3O_4 compounds exhibited acceptable catalytic activity (conversion in the range of 26–35%), however, all with 100% selectivity toward the annulation product **(4)**. It is interesting to see that no conversion of benzylamine could be detected over Ni-containing catalysts. To the best of our knowledge, the catalytic behavior of these non-supported 3d metal oxides for oxidative aniline couplings has not yet been reported in the literature.

3.2. Structural and analytical characterization of the modified bismutite structures

To build effective cooperative catalysts, the effect of the different synthesis strategies (Scheme 1) on the structure of the bismutite supported metal oxide composites were studied. XRD patterns of the samples synthesized by co-precipitation (Fig. 2./ a–d) and wet impregnation (Fig. 2./ e–g) are presented in Fig. 2, respectively. The Bragg reflections observed in the diffractograms can be associated with 00 *l*, 01 *l*,11 *l*, 02 *l* and 12 *l* series of Miller indices, corresponding to unit cell dimensions of pure carbonate-containing bismutite structure (PDF#41–1488) [57]. For co-precipitated samples, no other crystalline phases were observed. On the contrary, for the products obtained by the impregnation method, in addition to the reflections of the bismutite phase, intense reflections corresponding to the appropriate metal oxides can also be clearly identified; *i.e.,* Mn_3O_4 (PDF#24–0734) [58], Co_3O_4 (PDF#42–1467) [59] and NiO (PDF#47–1049) [60] that were crystallized as separate phases. The lack of these separated oxide phases in the diffractograms of the co-precipitated samples should be regarded as proof for the insertion of the transition metal specimens into the

Table 1
Oxidative coupling of benzylamine and 2-aminoaniline catalyzed by different bismuth compounds. (Reaction conditions: 1 equiv. (0.25 M) of benzylamine, 1.2 equiv. of 2-aminoaniline, DMSO (2 mL), 10 mol% of catalyst, 110 °C for 24 h).

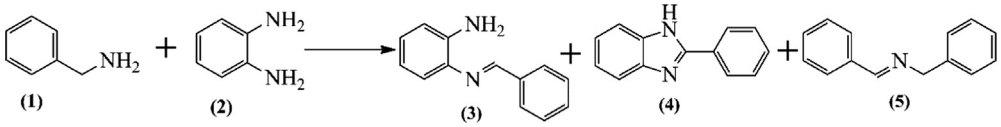

Bi-compounds	conversion of 1 (%)	selectivity of 3 (%)*	selectivity of 4 (%)**	selectivity of 5 (%)***
–	4 ± 1	–	–	100
$BiCl_3$	3 ± 2	–	–	100
BiI_3	4 ± 1	–	–	100
$Bi(NO_3)_3$	4 ± 2	–	–	100
BiOCl	2 ± 3	–	–	100
$NaBiO_3$	3 ± 4	–	–	100
Bi_2O_3	*11 ± 2*	11	9	80
$Bi_2O_2CO_3$	*19 ± 3*	18	5	77

* 2-(benzylideneamino)aniline.
** 2-phenylbenzimidazole.
*** benzyledenebenzylamine.

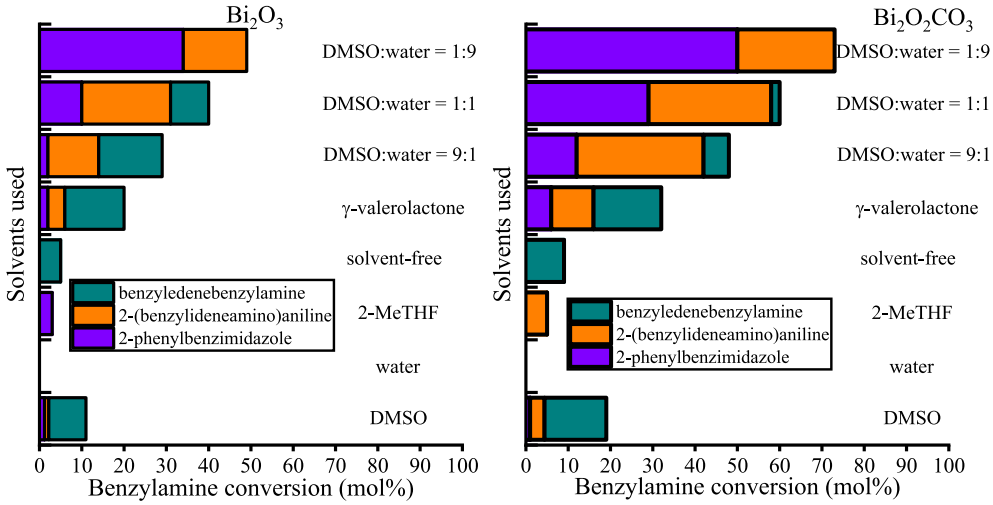

Fig. 1. Solvent effects in the oxidative coupling of benzylamine and 2-aminoaniline catalysed by different bismuth compounds. (reaction conditions: 1 equiv. (0.25 M) of benzylamine, 1.2 equiv. of 2-aminoaniline, **solvent** (2 mL), 10 mol% of catalyst, 110 °C (or reflux considering the boiling points) for 24 h).

Table 2
Oxidative coupling of benzylamine and 2-aminoaniline catalyzed by different transition metal compounds. (reaction conditions: 1 equiv. (0.25 M) of benzylamine, 1.2 equiv. of 2-aminoaniline, DMSO:H_2O 1:9 (2 mL), 10 mol% of catalyst, 100 °C for 24 h).

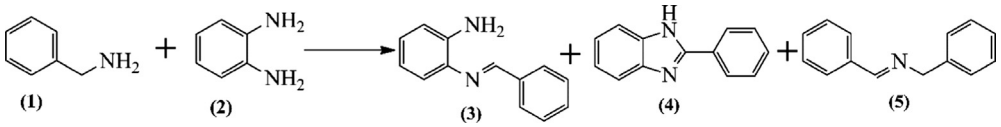

Catalysts	conversion of 1 (%)	selectivity of 3 (%)*	selectivity of 4 (%)**	selectivity of 5 (%)***
–	5 ± 1	–	–	100
MnO	2 ± 2	–	–	100
Mn_3O_4	31 ± 4	–	100	–
Mn_2O_3	–	–	–	–
MnO_2	26 ± 2	–	100	–
CoO	1 ± 1	–	–	100
$Co(OH)_2$	5 ± 3	–	–	100
Co_3O_4	35 ± 5	–	100	–
NiO	–	–	–	–
$Ni(OH)_2$	–	–	–	–
NiOOH	–	–	–	–
$Bi_2O_2CO_3$	*69 ± 4*	*27*	73	–

* 2-(benzylideneamino)aniline.
** 2-phenylbenzimidazole.
*** benzyledenebenzylamine, *italics: benchmark.*

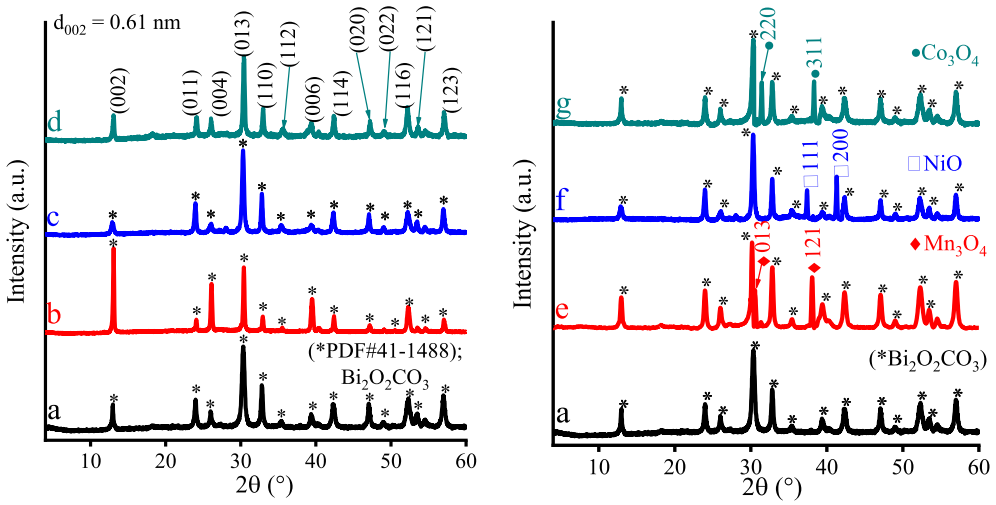

Fig. 2. XRD patterns of $Bi_2O_2CO_3$ (a), $MnBi_2O_2CO_3$ (b), $NiBi_2O_2CO_3$ (c), $CoBi_2O_2CO_3$ (d), Mn–$Bi_2O_2CO_3$ (e), Ni–$Bi_2O_2CO_3$ (f), Co–$Bi_2O_2CO_3$ (g). (co-precipitation: left side, wet impregnation: right side).

bismutite framework and/or the precipitation of oxide nanoparticles on the surface of the bismutite host. Nonetheless, it also means that during the impregnation procedure, transition metal oxides, most probably, could be anchored on the surface of the host by means of weak, intermolecular bonding (Scheme 1). Moreover, because all as-prepared samples exhibited an interlayer space of 0.61 nm, which is consistent with the interlamellar gallery of bismutite filled by carbonate ions, the intercalation of any specimen of transition metal ions could be excluded in all cases. Note that the alteration of the initial metal ion molar ratios led to significant changes in the crystalline phases during the optimization procedure (Fig. S1.) However, these changes are accompanied not only by the decrease in the crystallinity of the products but also by the appearance of undesired by-products that prevent even the formation of the bismutite framework resulting in indefinable amorphous structures. On the basis of our experience with the catalytic ability of bismuth-based catalysts presented above, the presence of the long-range ordered bismutite structure is essential to achieve effective coupling of anilines. Thus, further investigations shall focus on the well-defined bismutite structures. It should be noted that (for the impregnation method) more than one metal molar ratios proved to be useful for building well-defined bismutite structures. However, for comparability reasons, those ratios have been regarded as optimum which led to the formation of impregnated composites with almost the same metal ion molar ratios (see below) as in the case of their co-precipitated counterparts.

Elemental and chemical analyses confirmed that transition metal specimens were immobilized in/on the host bismutite during both synthesis procedures; however, in the solid products, the actual molar ratio of the transition metals and bismuth showed large variations depending on the quality of the guest molecules and the synthesis methods used. The bulk composition of the solid products (determined by combining ICP-MS and TG/DTG measurements) is shown in Table 3. Upon using exactly the same initial ratios of metal ions, for the impregnated samples, higher transition metal contents were found from the ICP-MS measurements, relative to the co-precipitated samples (Table 3 and Table S2). The affinity of the metal ions to be immobilized in/on the host yielded an order of Ni ≫ Mn > Co, independently of the synthesis procedure. It is interesting to note that the water/hydroxide-content of the solid samples displayed large variations. While, in comparison of pure bismutite structure, the water content of the co-precipitated Sillèn structures increased as a result of the nickel- as well as cobalt-insertion, no significant changes in the amount of inserted hydroxide was found, when manganese was used as dopant. According to the results shown in Table S3, the three impregnated samples do not present comparable amount of hydroxyl ions as well as no changes in the carbonate-content. Fig. S2 illustrates TG/DTG curves of the co-precipitated samples in which the number of the endothermic peaks varied with the guest molecules. For the pure bismutite and its manganese counterpart, there was only one endothermic peak at 470 °C in the DTG curves which is due to the decarboxylation of the structures. In parallel with the elimination of the interlayer carbonate and crystalline water (verified by TG-MS measurements), the collapse of the long-range-ordered structure and the formation of Bi_2O_3 and its doped analogue are possible to be detected. It can readily be seen that, after the collapse of the bismutite structure, beside characteristic reflections of pure bismuth oxide (PDF#4–294) (Fig. S3) [54], XRD patterns of $Bi_2Mn_4O_{10}$ (PDF#74–1096) [61] appear in the diffractogram of the doped analogue. For Ni- and Co-containing samples, similar observations can be made, however, with the appearance of the strongly bonded hydroxyl groups, exerting an effect on the thermal behavior of the solids. The total disintegration of the layered structure occurs in a two-step process. In the first step (~250–265 °C), the layered structure remains intact,

Table 3
Molar ratios of the metallic components and compositions of the as-prepared bismutite supported composites.

Composite	Initial Bi:M* ratio	Actual Bi:M* ratio	Bulk composition
$Bi_2O_2CO_3$	–	–	$(BiO)_2(CO_3)_{0.87}(OH)_{0.4}$
$Mn–Bi_2O_2CO_3$	0.5	7.8	$Mn_{0.26}O_{0.35}$/ $(BiO)_2(CO_3)_{0.85}(OH)_{0.60}$**
$Ni–Bi_2O_2CO_3$		3.1	$Ni_{0.64}O_{0.64}$/ $(BiO)_2(CO_3)_{0.89}(OH)_{0.55}$**
$Co–Bi_2O_2CO_3$		13.0	$Co_{0.15}O_{0.20}$/ $(BiO)_2(CO_3)_{0.83}(OH)_{0.58}$**
$MnBi_2O_2CO_3$	1.0	8.3	$Mn_{0.24}(BiO)_2(CO_3)_{1.05}(OH)_{0.35}$
$NiBi_2O_2CO_3$		3.0	$Ni_{0.66}(BiO)_2(CO_3)(OH)_{4.47}$
$CoBi_2O_2CO_3$		14.3	$Co_{0.14}(BiO)_2(CO_3)_{1.08}(OH)_{0.98}$

* M: Mn, Ni, Co; determined by ICP-MS.
** Oxygen-content of the transition metal oxides were inferred based on the XRD results.

and a phase transition occurs. This can be clearly confirmed by *ex situ* XRD study on these heat-treated samples (Fig. S3).

Fig. 3 together with Fig. S4 illustrate the results of the SEM-EDX analysis on the as-prepared solids. By impregnating the bismutite host, the corresponding EDX elemental mappings for Mn/Co/Ni elements confirmed a homogeneous spatial distribution of bismuth, which is in line with our previous hypothesis. Surprisingly, a heterogeneous dispersion of the cations could be observed on the EDX of the co-precipitated samples, this is in a slight contradiction with the XRD results.

To resolve this contradiction, TEM/TEM-EDX measurements (Fig. 4, Fig. S5 and S6) were carried out. TEM images verified that all co-precipitated samples consist of two types of nanoparticles with different morphologies as well as different dimensions. In all cases, smaller crystals of around 5–20 nm with spherical morphology were seen to sit directly on the top of the bigger (~300–600 nm), cubic crystals. The formation of large aggregates was detected that may cause the XRD patterns of the transition metal-containing particles with smaller dimensions to be hindered. This hypothesis could be further justified with TEM-EDX images. As can be seen, the smaller, spherical crystals are rich in the corresponding transition metals and oxygen, while the bigger ones are largely built around bismuth and oxygen, respectively. It could also be ascertained that transition metal-containing particles did not cover completely the surface of the bismuth-rich particles, as a result of the fact that the transition metal-based specimens were located separately in "island" structures.

Analysis of the far Raman shift region is a useful tool for the identification of the transition metal ion containing specimens (Fig. 5/A, C, E). Furthermore, upon using near-infrared laser power in this spectral region, bismutite host structure possess only three detectable Raman active modes at 358, 162 and 71 cm^{-1}, corresponding to the external vibrations of the $[Bi_2O_2]^{2+}$ layer and Bi–anion stretching mode vibration [54]. For impregnated samples, characteristic Raman modes of Mn_3O_4 [62], deformed (NiO or) Ni$(OH)_2$ [63] and Co_3O_4 [64] specimens could be identified which were attributed to the lattice mode vibrations of the oxides. This interpretation is fully in line with the XRD results shown in Fig. 2. Besides that, the characteristic Raman peaks of the host also appear in these spectra. For all composites, the complete peak assignment of Raman, UV–Vis and IR spectra can be found in Table S4. It should be noted that neither MnO_2 [62] nor CoO [64] have any Raman active vibration mode. Thus, the detection of these oxides is not possible with Raman spectroscopy. The formation of these non-Raman active oxides during the impregnation were excluded by XRD.

Regarding the co-precipitated samples, there are more significant changes in the Raman spectra relative to the host structure. First, the Raman peaks of the host structure disappeared or their intensities decreased significantly. This observation is due to the differences in the Raman scattering coefficient of the building blocks. Second, the intense characteristic peaks that appear in the presence of the corresponding metal ions cannot be assigned to Raman active modes of some well-known, commercial oxides or metallic particles. These bands are more possibly associated with the vibrations of Bi–O–M (M: Mn, Co) moieties [65], clearly illustrating the direct interaction between the host and the guests. These chemical bonds are most probably formed on the interfaces. However, taking into account the TEM results, there is no information about the quality of the transition metal species further away from the interfaces. This is a direct result of the application of near-IR laser source, providing bulk sensitive character for Raman detection.

The Ni-containing system is different from the Mn- and Co ones. Its Raman bands are readily attributed to deformed $Ni(OH)_2$ and bismutite components without giving rise to any other peaks, which is probably due to the lack of the Ni-bearing interfacial species. IR spectroscopy did not prove to be useful for providing

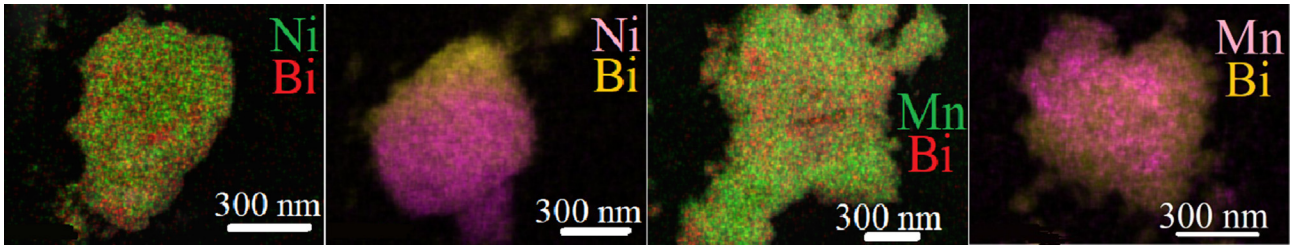

Fig. 3. SEM-EDX elemental maps of Ni- and Mn-based bismutite structures prepared by impregnation (green and red) or co-precipitation (pink and yellow) methods. (For interpretation of the references to colour in this figure legend, the reader is referred to the web version of this article.)

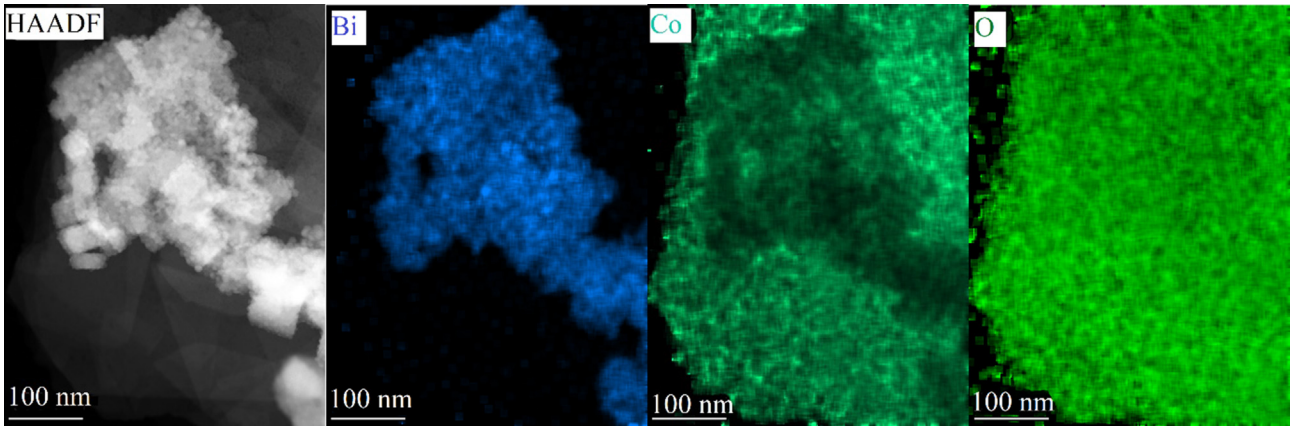

Fig. 4. HAADF TEM image and TEM-EDX elemental maps of $CoBi_2O_2CO_3$.

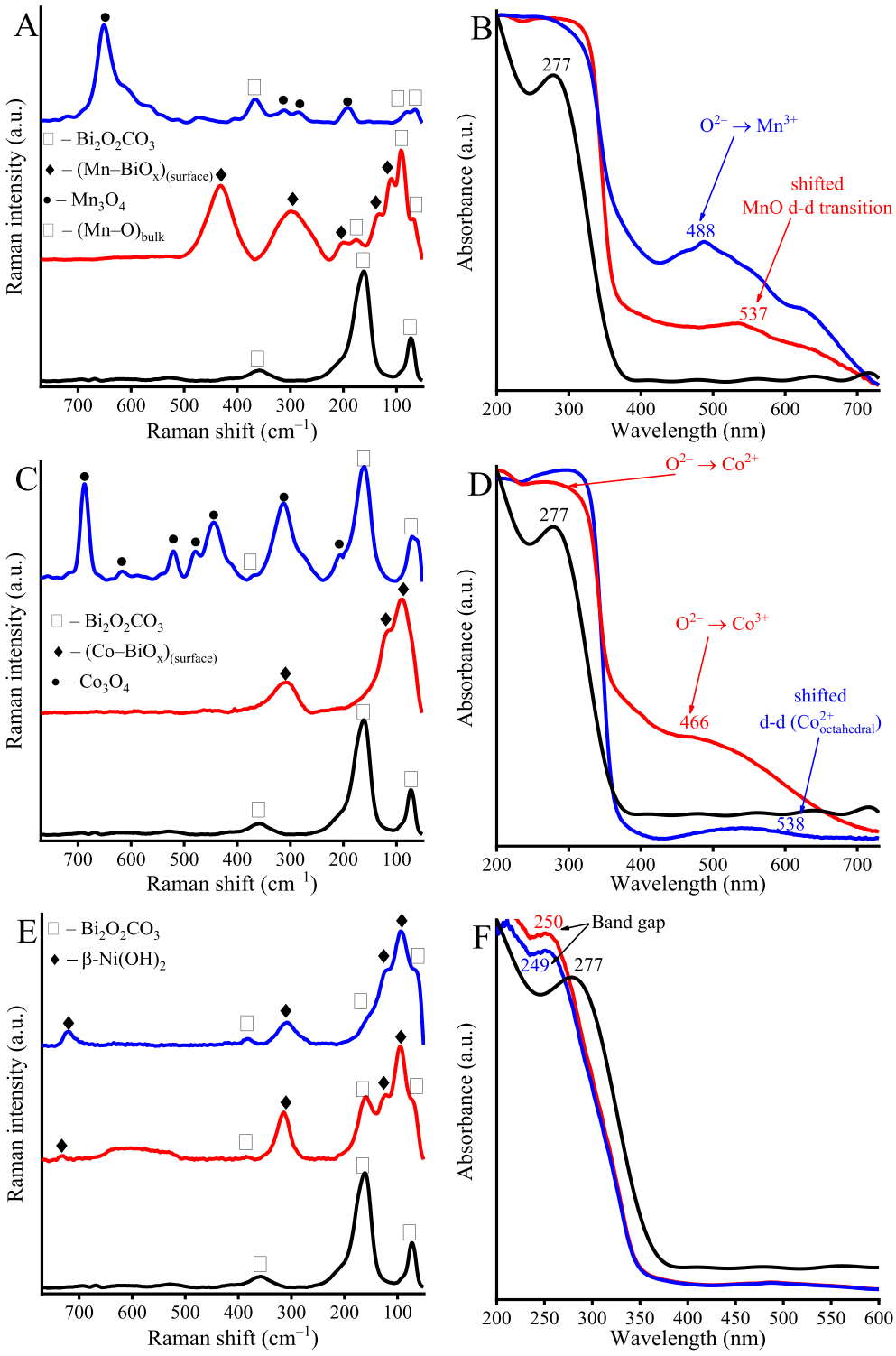

Fig. 5. Raman spectra (A, C, E) and UV-DRS spectra (B, D, F) of as-prepared $Bi_2O_2CO_3$ (black lines), $MBi_2O_2CO_3$ (red lines) and $M–Bi_2O_2CO_3$ (blue lines). (M: Mn, Co, Ni). (For interpretation of the references to colour in this figure legend, the reader is referred to the web version of this article.)

convincing information about the nature of the transition metal species (Fig. S7). Accordingly, anionic components other than carbonate and hydroxide cannot be inserted. Indeed, the IR bands at 3430–2500 cm^{-1} and 1670–1600 cm^{-1} correspond to the stretching and deformation mode vibrations of free and hydrogen bonded hydroxyl groups, respectively, while IR bands at 1420, 1397, 1046 and 840 cm^{-1} observed in all cases are due to carbonate compounds. Besides, relative to the pure bismutite, the intensity of the stretching mode vibrations of hydroxyl group become more dominant as a result of metal ion insertion processes. Moreover, considering the envelope of these vibration bands, it is also clear that significant amount of strongly bound hydroxyl groups are generated, upon using co-precipitation synthesis method. As a result of this, the peak of the free –OH groups (>3350 cm^{-1}) increase in intensity and broaden. This finding is in a good agreement with the interpretation of the TG/DTG curves.

The formation of the interfacial sites could be also verified by UV–Vis measurements (Fig. 5/B, D, F). As can be seen for the impregnated composites (*i.e.,* no interface effect), the absorption spectrum of the composites can be described as the linear combination of the transitions related to the bismutite and the corresponding transitions (mainly charge transfer ones [66–68]) of the 3d metal species. After recording the spectrum of the nickel-containing co-precipitated sample, exactly the same phenomenon could be observed, strengthening the hypothesis that there is no interfacial specimen in this case. On the contrary, for other co-precipitated samples, bathochromic shifts of the characteristic transitions of the metal species can be identified which is related to charge transfer, and are generated due to the presence of interfacing sites [69,70].

To investigate the surface transition metal specimens of the co-precipitated solids, XPS measurements were carried out (Fig. 6 and Fig. S8). XP spectra of the Bi 4f, Mn 2p, Co 2p and Ni 2p core levels of pure and transition metal modified bismutite samples are shown in Fig. 6. It can be seen that, for pure bismutite, the exact positions of Bi 4f bands and their separation of 5.3 eV illustrate the presence of the Bi(III) ions on the surface. The Bi 4f bands of the pure sample can be fitted *via* considering only one component (that is, without the need of peak deconvolution) at binding energies 164.1 and 158.8 eV; they can be attributed to Bi(III) species incorporated into a Sillèn-type bismutite framework [71]. By modifying the bismutite framework with manganese and cobalt ions, these characteristic bands are shifted to higher binding energies and a broadening of these peaks are also clearly observed after the modification. These changes are due to the appearance of the interfacial specimens. This hypothesis is further supported by considering the lack of these changes in the spectrum of the nickel-containing sample. Bi 4f bands of this composite are almost identical with that of the pure bismutite what indicates the absence of the interfacial species. This assignment is in line with the interpretation of the Raman and UV–Vis measurements. Furthermore, the 2p bands of manganese and cobalt of the modified samples can be described with only one component, corresponding to MnO and $Co(OH)_2$, respectively [72]. Accordingly, Mn(II) and Co (II) ions can occupy the right positions on the surface of the composite exclusively. For nickel-bismutite system, there is no identical chemical environments of nickel which can be identified and some kind of unidentifiable linear combination of NiO, $Ni(OH)_2$ and NiOOH species can be found on the surface of this sample [73]. In addition, two different components should be considered for the right description of this curve which are independent of each other. Other (oxygen, carbon) components of the spectra could be described as almost identical surface species of the bismutite host (Fig. S8).

At this point, it can be stated that the immobilization of well-characterized pure oxide specimens on the surface of bismutite host can be obtained by means of two different synthesis methods. Wet impregnation method and the nickel-based co-precipitation led to the formation of surface modified bismutite structure in which the transition metal specimens are linked to the surface of

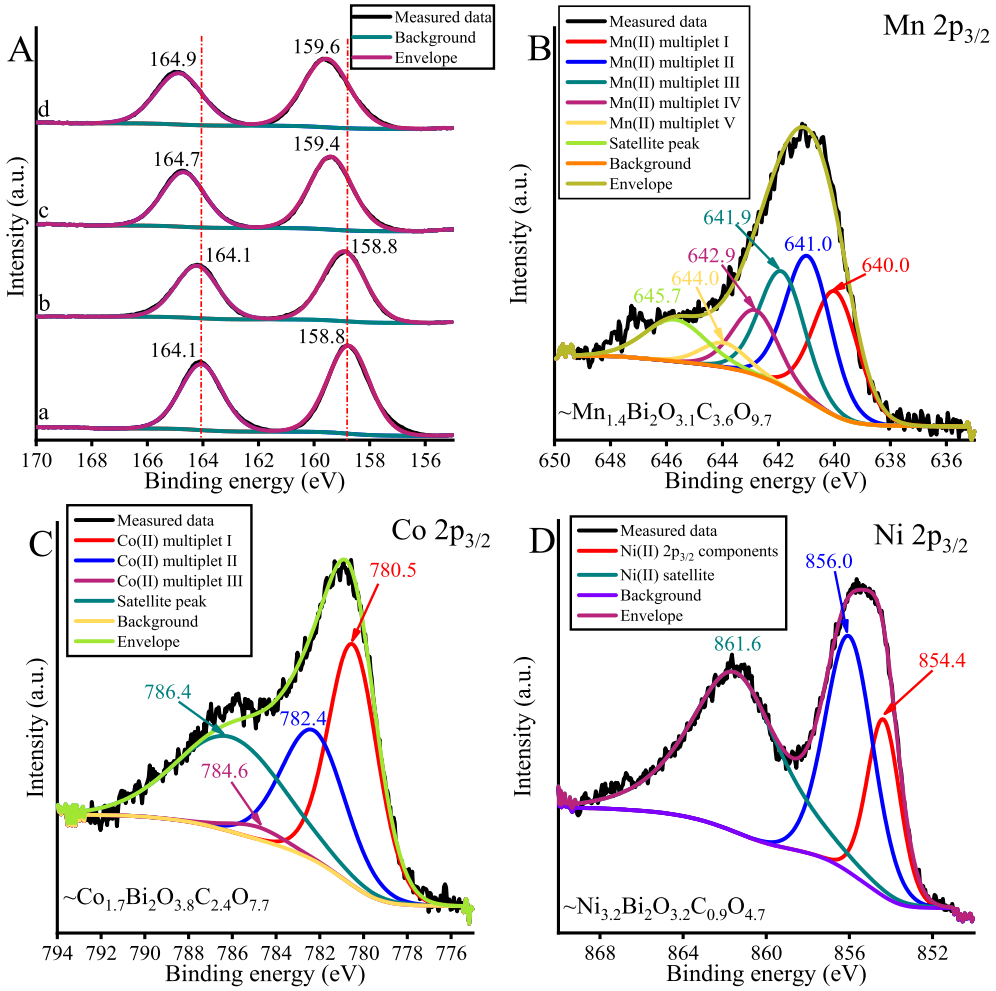

Fig. 6. Bi 4f (A), Mn $2p_{3/2}$ (B), Co $2p_{3/2}$ (C) and Ni $2p_{3/2}$ (D) XP spectra of the as-prepared $MBi_2O_2CO_3$ (M: none, Mn, Co, Ni).

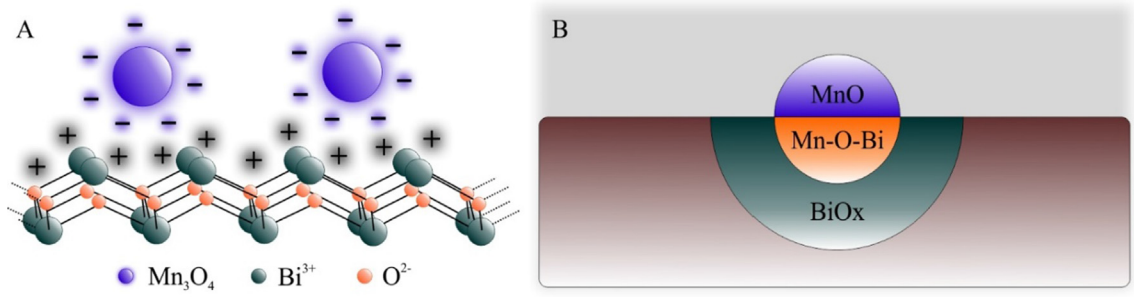

Scheme 3. Illustrative side views of the as-prepared bismutite-supported manganese oxides produced *via* wet impregnation (A) or co-precipitation method (B).

the host *via* weak interactions (Scheme 3/A). For the two further co-precipitated samples, a well detectable portion of M−BiO_X interfacial sites can be identified, demonstrating a strong interaction between the host and the guest molecules (Scheme 3/B).

3.3. Catalytic behavior of the modified bismutite structures

With the as-prepared, well-characterized composite materials in our hand, their catalytic ability was then probed in the oxidative transformation of benzylamine (Fig. 7 and Fig. S9). Optimization procedure was performed, using the co-precipitated samples. Hence, by altering the solvent used (Fig. 7), it was revealed that benzylamine was efficiently converted by means of the robust manganese- and cobalt-containing catalysts that display significant tolerance towards numerous organic solvents as well as water. The best operation was experienced in DMSO:H_2O 1:9 mixture in both cases ($MnBi_2O_2CO_3$: ~95% conversion/~97% selectivity, $CoBi_2O_2CO_3$: ~96% conversion/~95% selectivity). Compared with our benchmark catalyst (~69% conversion, ~73% selectivity in DMSO:H_2O 1:9 mixture), a profound effect of the inserted 3d metal species on the catalytic activity of the bismutite host was observed, causing significant enhancement in the benzylamine conversions, independently of the solvents used. Additionally, in the presence of the dopants, the desired products were obtained with excellent levels of chemoselectivity that approximated the unique 2-phenylbenzimidazole **(4)** selectivity obtained for pure metal oxides (see above). Moreover, in γ-valerolactone, 100% selectivity toward the annulation product **(4)** was realized by means of the cobalt-bismuth catalyst. In addition, the use of acetonitrile:water 1:1 solvent mixture enabled the exclusive formation of 2-(benzylideneamino)aniline **(3)**, presenting a facile way of controlling the product distribution over the active catalyst. The key importance of the quality of the 3d metal ions became evident through a set of optimization reactions that involved studies on both the catalyst-loading- and temperature-dependence of the oxidative transformation (Fig. S9). The Co(II)-based catalyst gave good results with a catalyst loading as low as 2.5 mol%, whilst 10 mol% of the Mn(II)-containing bismutite catalyst was required to reach high level of 2-phenylbenzimidazole **(4)** formation. Both catalysts performed best at reaction temperatures ≥ 90 °C.

The significant transition metal-dependence of the catalytic reaction was also supported by the fact that all the alternative, Ni-based catalysts prepared by us were found to be completely ineffective without any exemption (not shown), similarly to pure NiO (see above). This observation should be regarded as a marker of the main role of the surface anchored metal specimens that necessarily dictates the co-catalytic feature of the Bi(III) centers.

To further investigate the role of the interfacial species and the cooperative catalytic features of the composites, impregnated bismutites were involved in the tests for comparison (Fig. 8). On one hand, by carrying out the test reaction under the optimized reaction conditions in the presence of the catalysts made by impregnation, supported transition metal specimens exhibited much better catalytic performance than those that were not anchored on the bismutite surface. This indicates that Bi(III)-centers participate directly in the oxidative transformations. Accordingly, it has been suggested that the co-presence of the active transition metal species and the bismuth centers facilitates the organic transformation,

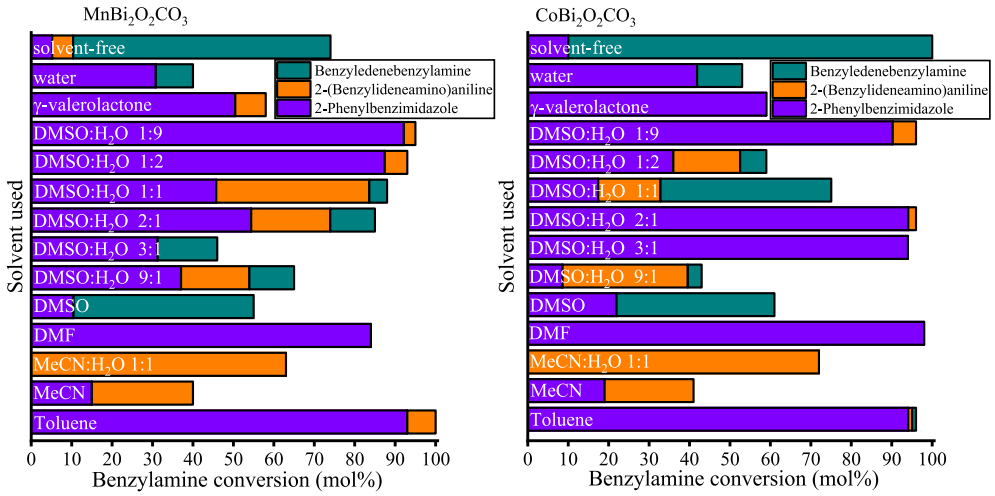

Fig. 7. The effect of various solvents in the oxidative coupling of benzylamine and 2-aminoaniline. Reaction conditions: 1 equiv. (0.25 M) of benzylamine, 1.2 equiv. of 2-aminoaniline, 10 mol% of $MnBi_2O_2CO_3$ (**left side**) and $CoBi_2O_2CO_3$ (**right side**), 110 °C (100 °C: DMSO:water mixtures, water; reflux: MeCN-containing solvents) for 24 h.

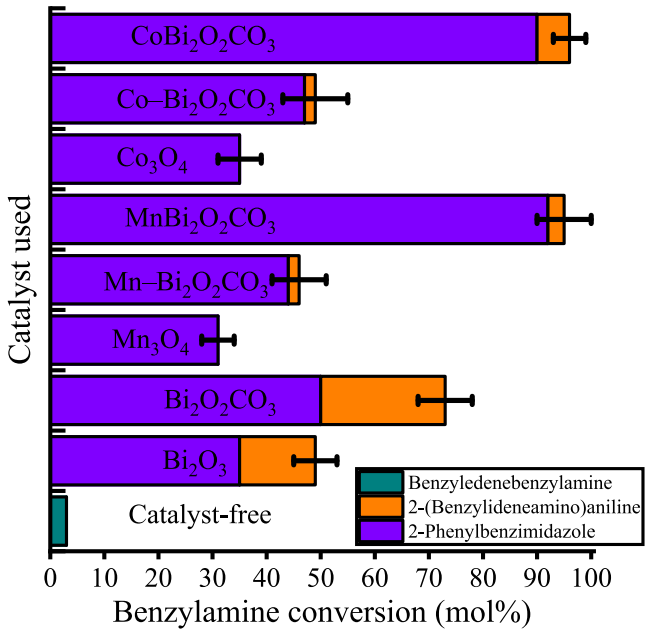

Fig. 8. The effect of the quality of the catalysts in the oxidative coupling of benzylamine and 2-aminoaniline. Reaction conditions: 1 equiv. (0.25 M) of benzylamine, 1.2 equiv. of 2-aminoaniline, DMSO:H_2O 1:9 (2 mL), 10 mol% of catalyst, 100 °C for 24 h. ($MBi_2O_2CO_3$: co-precipitated samples; $M–Bi_2O_2CO_3$: impregnated samples.)

acting as cooperative catalysts. On the other hand, it has also been found that these impregnated materials showed substantially decreased activity, with selectivity similar to that of their counterparts obtained by co-precipitation. Indeed, there is a clear correlation between the presence of each of interfacial species and the catalytic activity during the oxidative transformations.

To quantify the above-mentioned difference in the activity of the active centers and to investigate the kinetic profile of the catalytic reaction, the time-dependence of the oxidative transformations have also been investigated. All kinetic curves of the active catalysts and turnover frequency (TOF) values – calculated from the initial reaction rates as the number of molecules transformed per hour and per metal ions – are shown in Fig. 9. The maximum yield of the desired 2-phenylbenzimidazole product **(4)** increased continuously (for *ca.* 24 h) up to 93%, 92%, 46% and 44% over $MnBi_2O_2CO_3$, $CoBi_2O_2CO_3$, $Mn–Bi_2O_2CO_3$, $Co–Bi_2O_2CO_3$ catalysts, respectively. However, within only 8 h, the maximum yield of 88% could be achieved by using the $CoBi_2O_2CO_3$ composite. From these results it can also be concluded that cobalt-containing samples gave much higher TOFs than their manganese-based counterparts. It should be noted that the TOF of co-precipitated samples were almost 4-times larger than those of the corresponding impregnated ones clearly indicating the positive effect of the interfacial specimens generated during co-precipitation. Finally, from the comparison of the TOF values it can be concluded that neither the Bi(III) nor the 3d metal ion centers function as the active sites by themselves as there are really high differences in the initial activity of the bismutite supported catalysts. Indeed, cooperative catalytic features are possible to be related to the as-prepared composites. It is interesting to note that, in γ-valerolactone as solvent, the TOF values for the co-precipitated samples were found very high, however, the selectivities and maximum yields were lower Fig. S10.

After demonstrating that Bi(III)/TMOs-based composites efficiently promote the oxidative conversion of benzylamine, we investigated in detail how each part functions in the individual reaction steps on which the reaction sequence was built.

To do this, the catalytic ability of pure Co_3O_4 (cobaltite) and $Bi_2O_2CO_3$ (bismutite) samples as well as the Co-based cooperative catalyst was tested as a function of time in both the oxidation reaction of benzylamine and its oxidative coupling with 2-aminoaniline (Fig. 10). In the absence of 2-aminoaniline, the commercial inorganics showed moderate activity with exclusive selectivity for the product benzyledenebenzylamine. However, the calculated TOFs showed that the cobalt species had higher activity in this reaction. The cooperative catalyst possessed higher activity with the same selectivity as its individual building blocks. The observed selectivities were due to the known instability/reactivity of the benzylamine [74]. Despite all attempts, this phenomenon made it impossible to study the oxidative coupling of benzylimine independently. Instead of this approach, building blocks have been studied in the coupling/annulation of benzylamine with 2-aminoaniline. While 2-phenylbenzimidazole was produced almost exclusively with the bismutite catalyst, every possible product was detected when the reaction was carried out with cobaltite, but their distribution varied over time. This probably means that the reaction rate of conversion of benzylimine to 2-(benzylideneamino)aniline is higher when the bismuthite catalyst is used than when the reaction is catalysed by cobaltite.

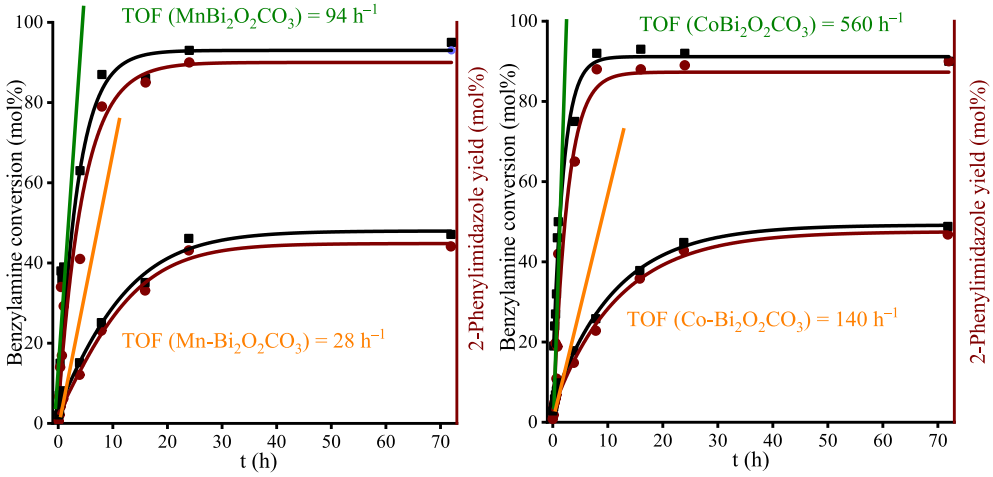

Fig. 9. Conversions of benzylamine and yields of 2-phenylbenzimidazole as a function of time in the oxidative coupling of benzylamine and 2-aminoaniline catalyzed by $MnBi_2O_2CO_3$ (**left side**) and $CoBi_2O_2CO_3$ (**right side**) catalysts. Reaction conditions: 1 equiv. (0.25 M) of benzylamine, 1.2 equiv. of 2-aminoaniline, DMSO:H_2O 1:9 (2 mL), 10 mol% of $MnBi_2O_2CO_3$ or 2.5 mol% of $CoBi_2O_2CO_3$, 90 °C (**left side**)/100 °C (**right side**).

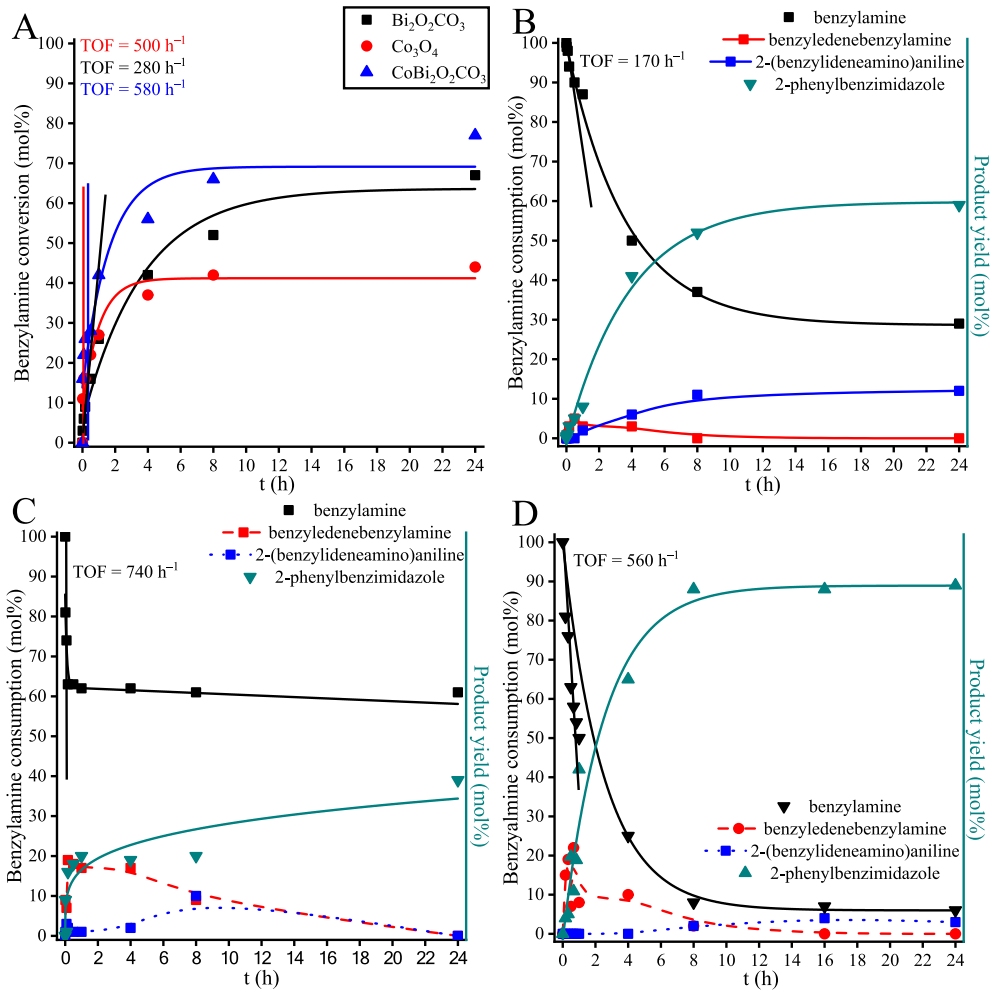

Fig. 10. Benzylamine conversion as a function of time in the oxidation reaction of benzylamine catalyzed by $CoBi_2O_2CO_3$, $Bi_2O_2CO_3$ and Co_3O_4 catalysts (**A**). Reaction conditions: 1 equiv. (0.25 M) of benzylamine, DMSO:H_2O 1:9 (2 mL), 2.5 (**D**)/10 mol% (**B, C**) of catalyst, 100 °C. Consumption of benzylamine and product distribution as a function of time in the oxidative coupling/annulation of benzylamine and 2-aminoaniline catalyzed by $Bi_2O_2CO_3$ (**B**), Co_3O_4 (**C**) and $CoBi_2O_2CO_3$ (**D**) catalysts. Reaction conditions: 1 equiv. (0.25 M) of benzylamine, 1.2 equiv. of 2-aminoaniline, DMSO:H_2O 1:9 (2 mL), 2.5 (**D**)/10 mol% (**B, C**) of catalyst, 100 °C.

Nevertheless, the consumption rate (TOF) of benzylamine was higher in the cobalt-catalyzed reaction than in the bismutite-promoted reaction. In the case of cooperative catalysis, a similar product distribution was observed as in bismutite catalysis, but the consumption rate of benzylamine observed was similar to that of cobaltite. By taking into account all above results, it can be supposed that the rate-controlling step of the reaction sequence corresponds to the oxidation of benzylamine that may take place at the cobalt-oxide centres on the surface of the cooperative catalysts, considering the trend in the TOFs determined. Furthermore, in the case of the composite catalyst, the coupling/annulation step (s) would take place on the bismutite specimens.

After the oxidative transformations, active Mn- and Co-based catalysts were separated from the reaction mixture by centrifugation followed by thorough washing steps using ethanol, water and DMSO as well as their mixtures for purification. The separated and washed samples were reutilized as catalysts in following runs under the optimized reaction conditions. Upon using co-precipitated samples, there was no significant decrease in the benzylamine conversions for up to five runs (Fig. 11). The results also indicated that after the first cycle the product distribution between the oxidative coupling **(3)** and oxidative annulation **(4)** products significantly changed and then reached a plateau value at around 2-phenylbenimidazole **(4)** selectivity of 65% in both cases in the third cycle. Moreover, neither measurable leaching of any metallic components (ICP-MS) nor structural changes in the isolated samples (XRD) from the fifth catalytic run could be identified any of which would provide potential explanations for the changes in the selectivity. However, *ex situ* XRD analysis also revealed that the crystallinity of the host slightly decreased at the end of the third catalytic run which may explain the mentioned changes in selectivity by hindering the access of some of the active sites (Fig. S11). In case of the application of the impregnated samples, after three successive cycles the catalytic activity of the composites decreased significantly (benzylamine conversion 13%, Fig. S12) and redistribution of the products was observed. These are mainly due to the leaching of the 3d metal-containing specimens as confirmed by both ICP-MS and XRD analysis (Fig. S11). This quick degradation led to the total washing out of both the manganese- and cobalt-content from the samples at the end of the third cycle. This is probably because of the heterogenization mode that gives in these cases weakly bonded 3d transition metal specimens on the surface of the bismutite host and enables leaching of the transition metal components without collapse of the host. Hot filtration experiments showed that the oxidative transformation kept going after the removal of the impregnated catalysts while those where co-precipitated samples were used were stopped by the catalyst removal (Fig. S13). In this latter case, the product distribution was unchanged over time even after the catalysts were removed. Accordingly, the heterogeneous nature of the reactions promoted

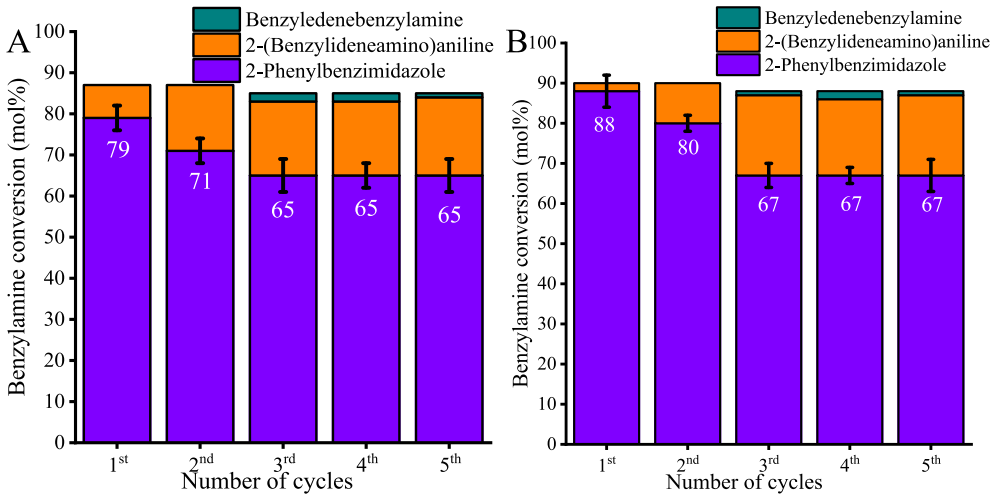

Fig. 11. Reusability of $MnBi_2O_2CO_3$ (**A**) and $CoBi_2O_2CO_3$ (**B**) in the oxidative coupling of benzylamine and 2-aminoaniline. Reaction conditions: 1 equiv. (0.25 M) of benzylamine, 1.2 equiv. of 2-aminoaniline, DMSO:H_2O 1:9 (2 mL), 10 mol% of $MnBi_2O_2CO_3$ or 2.5 mol% of $CoBi_2O_2CO_3$, 90 °C (**A**) or 100 °C (**B**) for 8 h.

Table 4
Scope of N-, O- and S-containing heterocycles production *via* oxidative coupling of benzylamine-derivatives and 2-amino /hydroxy /mercapto anilines over $MnBi_2O_2CO_3$ and $CoBi_2O_2CO_3$ catalysts.

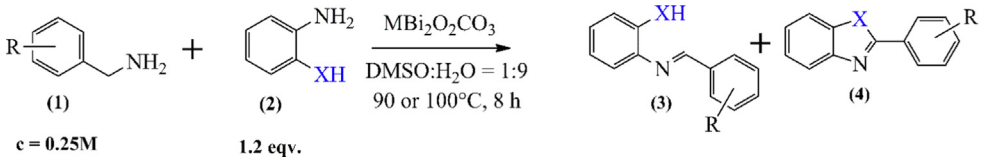

		$MnBi_2O_2CO_3$ (90 °C)			$CoBi_2O_2CO_3$ (100 °C)		
#	**X = NH**	**conversion of 1 (%)**	**selectivity of 3 (%)[1]**	**selectivity of 4 (%)[2]**	**conversion of 1 (%)**	**selectivity of 3 (%)[1]**	**selectivity of 4 (%)[2]**
1	R = *p*-OMe	57	88	12	57	48	52
		93*	33*	67*	97*	20*	80*
2	R = *o*-OMe	72	64	36	43	0	100
		99*	17*	83*	79*	0*	100*
		76**	59**	39**	48**	0**	92**
3	R = *p*-Cl	73	84	16	68	74	26
		100*	23*	77*	91*	19*	81*
4	R = *o*-Cl	80	73	23	68	82	18
		100*	15*	85*	95*	23*	77*
5	R = *m*-nitro	71	0	100	76	0	100
		100*	0*	100*	100*	0*	100*
#	**X = O**	**conversion of 1 (%)**	**selectivity of 3 (%)[1]**	**selectivity of 4 (%)[2]**	**conversion of 1 (%)**	**selectivity of 3 (%)[1]**	**selectivity of 4 (%)[2]**
1	R = H	100	70	30	23	0	100
2	R = *p*-OMe	59	46	54	69	19	81
		100*	19*	81*	100*	6*	94*
3	R = *o*-OMe	75	80	20	47	0	100
4	R = *p*-Cl	37	73	27	19	37	63
5	R = *o*-Cl	57	49	51	95	63	37
6	R = *m*-nitro	91	94	6	100	86	14
#	**X = S**	**conversion of 1 (%)**	**selectivity of 3 (%)[1]**	**selectivity of 4 (%)[2]**	**conversion of 1 (%)**	**selectivity of 3 (%)[1]**	**selectivity of 4 (%)[2]**
1	R = H	37	68	32	88	43	57
2	R = *p*-OMe	52	46	54	17	53	47
		99*	22*	78*	45*	33*	67*
3	R = *o*-OMe	79	80	20	50	0	100
4	R = *p*-Cl	31	77	23	68	50	50
5	R = *o*-Cl	74	99	1	62	0	100
6	R = *m*-nitro	39	100	0	83	99	1

[1] cross-coupled imines and their isosteres.
[2] benzimidazoles and their isosteres.
* subsequent reactions: Mn: 90 °C for 8 h + 110 °C for 4 h and Co: 100 °C for 8 h + 110 °C for 4 h.
** subsequent reactions without catalysts.

by $CoBi_2O_2CO_3$ and $MnBi_2O_2CO_3$ have been proven. Taking into account the high catalytic activity and recyclability of the co-precipitated cooperative catalytic systems, it can be revealed that these materials are competitive and attractive oxidative coupling/annulation catalysts compared to benchmark catalysts reported earlier (see Table S1). By using bismutite-based coopera-

tive catalysts, high reaction rates and excellent chemical selectivities were achieved under mild reaction conditions (t = 8 h, T = 90 °C, ambient air as oxidant) and in environmentally-reliable solvents (DMSO:H_2O 1:9 or γ-valerolactone). Moreover, no additives or inorganic bases were necessary and the heterogeneous catalysts could readily be reused and recycled.

Importantly, both cooperative catalysts showed high versatility to promote oxidative transformations of diversely substituted anilines and benzylamines (Table 4). In most of the cases, under the well-established reaction conditions, catalytic processes offered the oxidative coupling product with high selectivity (64–88 %) and good conversion (37–100 % after 8 h) without the appearance of the undesired self-coupling product of the benzylamines. In cases of *ortho*-methoxy- and *meta*-nitro-substituted benzylamines, exclusive formation of the corresponding annulation product was detected. Importantly, the manganese(II) and cobalt(II) catalysts were not limited to 2-aminoaniline couplings. 2-Aminophenols as well as 2-aminobenzenethiols were readily transformed in the presence of various substituted benzylamines under similar reaction conditions affording the corresponding benzoxazoles and benzothiazoles.

The selectivity results may further indicate that the catalytic ring-closing reaction step for the production of benzimidazole derivatives and their isosteres were substantially controlled by the reaction temperature used. To verify our hypothesis, a temperature-programmed reaction sequence was then introduced. Repeating the reactions in such a way that the 8-hour-long step at 90 (Mn-based catalysts)/100 °C (Co-based catalysts) was followed subsequently by a 4-hour-long step at 110 °C, the ring-closing also took place, providing the annulation products. It should be noted that at 110 °C, practically pure DMSO as a solvent was left behind at the end of the reaction. Indeed, by numerous benzylamine analogues, both oxidative coupling product and oxidative annulation product could be produced with controlling the selectivity by the temperature program. To exclude the possibility for occurring the ring-closing *via* (non-catalytic) thermal way, in some cases, this second step was rerun after the elimination of the catalysts from the reaction mixtures. Thereby, there were no significant changes in either in the conversions or in the selectivities compared with the original ones, reflecting the catalytic character of this second step.

4. Conclusions

From the results presented herein, it can be concluded that Lewis acid sites of the Sillèn-type bismutite framework are effectively promoting the oxidative cross coupling and/or oxidative annulation reactions of anilines with amines. This bismutite structure is the first reported bismuth-based compound with heterogeneous features that is able to promote oxidative CH/NH annulations, with avoiding the undesired homocoupling of benzylamines. Commercial transition metal oxides, especially cobalt and manganese oxides with well-defined stoichiometry (*i.e.,* MnO_2, Mn_3O_4 and Co_3O_4) were also found to be useful for oxidative transformations exhibiting exclusive selectivity for annulation products. To build cooperative catalysts that outperform the catalytic efficacy of its building blocks, wet impregnation and co-precipitation were then introduced which provided hierarchically ordered (nano)composite structures, having anchored metal oxide species (Ni(II), Mn(II), Co(II)) immobilized *via* interactions of different strengths on the bismutite surface. More probably, weak, electrostatic bindings have evolved between transition metal oxides and the surface upon using impregnation method while co-precipitation led to the formation of strongly bonded oxides on the surface of the host. To this latter interaction, the generation of the interfacial sites (identified by spectroscopic technique) could contribute. On the interface, Bi–O–M−like (where M is a 3d metal) specimens were generated during the co-precipitation. By applying the as-prepared composites as catalysts, a useful combination of the catalytic ability of the building blocks was observed, giving a significant increase both in the conversions and in product selectivities. Besides the main role of the surface anchored metal oxides, the cooperative features of the Lewis acid and charge valuable sites could be also demonstrated, creating first cooperative Lewis acid/-transition metal catalyzed C–H/N–H annulations. By generating the interfacial sites, the catalytic activity and the selectivity of the composites could be further enhanced without changes in the stability of the catalysts. By systematically altering the solvents and/or the reaction sequence used, selective formation of cross-coupled imines and benzimidazoles were achieved. 2-Aminophenols as well as 2-aminobenzenethiols were also readily transformed resulting valuable benzoxazoles and benzothiazoles. The 3d metal oxide nanoparticles that interact strongly with bismutite surface (resulting in $MnBi_2O_2CO_3$ and $CoBi_2O_2CO_3$) proved to be recyclable. These compounds could function under mild reaction conditions in environmentally-reliable solvents in the presence of ambient air as the simplest possible oxidant.

Declaration of Competing Interest

The authors declare that they have no known competing financial interests or personal relationships that could have appeared to influence the work reported in this paper.

Appendix A. Supplementary data

Supplementary data to this article can be found online at https://doi.org/10.1016/j.jcat.2022.09.008.

References

[1] G. Yadav, S. Ganguly, Structure activity relationship (SAR) study of benzimidazole scaffold for different biological activities: A mini-review, Eur. J. Med. Chem. 97 (2015) 419–443, https://doi.org/10.1016/j.ejmech.2014.11.053.
[2] D. Mahesh, P. Sadhu, T. Punniyamurthy, Copper(II)-Catalyzed Oxidative Cross-Coupling of Anilines, Primary Alkyl Amines, and Sodium Azide Using TBHP: A Route to 2-Substituted Benzimidazoles, J. Org. Chem. 81 (2016) 3227–3234, https://doi.org/10.1021/acs.joc.6b00186.
[3] E. Vitaku, D.T. Smith, J.T. Njardarson, Analysis of the structural diversity, substitution patterns, and frequency of nitrogen heterocycles among U.S. FDA approved pharmaceuticals, J. Med. Chem. 57 (2014) 10257–10274, https://doi.org/10.1021/jm501100b.
[4] S. Riera-Galindo, A. Orbelli Biroli, A. Forni, Y. Puttisong, F. Tessore, M. Pizzotti, E. Pavlopoulou, E. Solano, S. Wang, G. Wang, T.P. Ruoko, W.M. Chen, M. Kemerink, M. Berggren, G. Di Carlo, S. Fabiano, Impact of Singly Occupied Molecular Orbital Energy on the n-Doping Efficiency of Benzimidazole Derivatives, ACS Appl. Mater. Interfaces. 11 (2019) 37981–37990, https://doi.org/10.1021/acsami.9b12441.
[5] Z. Ge, T. Hayakawa, S. Ando, M. Ueda, T. Akiike, H. Miyamoto, T. Kajita, M. Kakimoto, Spin-coated highly efficient phosphorescent organic light-emitting diodes based on bipolar triphenylamine-benzimidazole derivatives, Adv. Funct. Mater. 18 (2008) 584–590, https://doi.org/10.1002/adfm.200700913.
[6] P.S. Salunkhe, Y.S. Patil, I.A. Dhole, B.S. Kalshetti, V.B. Patil, S.R. Mane, A.A. Ghanwat, A novel synthetic approach for designing metal-free, redox-active quinoxaline-benzimidazole-based organic polymers with high energy storage capacity, New J. Chem. 43 (2019) 14806–14817, https://doi.org/10.1039/c9nj02877c.
[7] D.D. Medina, T. Sick, T. Bein, Photoactive and Conducting Covalent Organic Frameworks, Adv. Energy Mater. 7 (2017) 1–8, https://doi.org/10.1002/aenm.201700387.
[8] S. Anbu, A. Paul, K. Surendranath, N.S. Solaiman, A.J.L. Pombeiro, A benzimidazole-based new fluorogenic differential/sequential chemosensor for Cu^{2+}, Zn^{2+}, CN^-, $P_2O_7^{4-}$, DNA, its live-cell imaging and pyrosequencing applications, Sensors Actuators, B Chem. 337 (2021), https://doi.org/10.1016/j.snb.2021.129785 129785.
[9] M. Li, H. Ge, R.L. Arrowsmith, V. Mirabello, S.W. Botchway, W. Zhu, S.I. Pascu, T. D. James, Ditopic boronic acid and imine-based naphthalimide fluorescence sensor for copper(II), Chem. Commun. 50 (2014) 11806–11809, https://doi.org/10.1039/c4cc03453h.

[10] Y. Chen, L. Qian, W. Zhang, B. Han, Efficient Aerobic Oxidative Synthesis of 2-Substituted Benzoxazoles, Benzothiazoles, and Benzimidazoles Catalyzed by 4-Methoxy-TEMPO, Angew. Chem. Int. Ed. 47 (2008) 9330–9333, https://doi.org/10.1002/anie.200803381.
[11] R. Trivedi, S.K. De, R.A. Gibbs, A convenient one-pot synthesis of 2-substituted benzimidazoles, J. Mol. Catal. A Chem. 245 (2006) 8–11, https://doi.org/10.1016/j.molcata.2005.09.025.
[12] D.K. Maiti, S. Halder, P. Pandit, N. Chatterjee, D. De Joarder, N. Pramanik, Y. Saima, A. Patra, P.K. Maiti, Synthesis of glycal-based chiral benzimidazoles by $VO(acac)_2$-$CeCl_3$ combo catalyst and their self-aggregated nanostructured materials, J. Org. Chem. 74 (2009) 8086–8097, https://doi.org/10.1021/jo901458k.
[13] M. Boronat, A. Corma, M. Renz, Mechanism of the Meerwein - Ponndorf - Verley - Oppenauer (MPVO) redox equilibrium on Sn- and Zr - Beta zeolite catalysts, J. Phys. Chem. B. 110 (2006) 21168–21174, https://doi.org/10.1021/jp063249x.
[14] J.M. Bothwell, S.W. Krabbe, R.S. Mohan, Applications of bismuth(III) compounds in organic synthesis, Chem. Soc. Rev. 40 (2011) 4649–4707, https://doi.org/10.1039/c0cs00206b.
[15] D. Wang, J. Albero, H. García, Z. Li, Visible-light-induced tandem reaction of o-aminothiophenols and alcohols to benzothiazoles over Fe-based MOFs: Influence of the structure elucidated by transient absorption spectroscopy, J. Catal. 349 (2017) 156–162, https://doi.org/10.1016/j.jcat.2017.01.014.
[16] A. Bermejo-López, S. Carrasco, P.J. Tortajada, K.P.M. Kopf, A. Sanz-Marco, M.S. Hvid, N. Lock, B. Martín-Matute, Selective Synthesis of Imines by Photo-Oxidative Amine Cross-Condensation Catalyzed by PCN-222(Pd), ACS Sustainable Chem. Eng. 9 (2021) 14405–14415, https://doi.org/10.1021/acssuschemeng.1c04389.
[17] C. Su, R. Tandiana, J. Balapanuru, W. Tang, K. Pareek, C.T. Nai, T. Hayashi, K.P. Loh, Tandem catalysis of amines using porous graphene oxide, J. Am. Chem. Soc. 137 (2015) 685–690, https://doi.org/10.1021/ja512470t.
[18] G. Naresh, R. Kant, T. Narender, Molecular Iodine Promoted Divergent Synthesis of Benzimidazoles, Benzothiazoles, and 2-Benzyl-3-phenyl-3,4-dihydro-2H -benzo[e][1,2,4]thiadiazines, J. Org. Chem. 79 (2014) 3821–3829, https://doi.org/10.1021/jo5000797.
[19] K. Yamaguchi, N. Mizuno, Efficient heterogeneous aerobic oxidation of amines by a supported ruthenium catalyst, Angew. Chem. Int. Ed. 42 (2003) 1480–1483, https://doi.org/10.1002/anie.200250779.
[20] R.J. Angelici, Bulk gold (non-nanogold) catalysis of aerobic oxidations of amines, isocyanides, carbon monoxide, and carbene precursors, Catal. Sci. Technol. 3 (2013) 279–296, https://doi.org/10.1039/c2cy20348k.
[21] R. Brišar, F. Unglaube, D. Hollmann, H. Jiao, E. Mejía, Aerobic oxidative homo- and cross-coupling of amines catalyzed by phenazine radical cations, J. Org. Chem. 83 (2018) 13481–13490, https://doi.org/10.1021/acs.joc.8b02345.
[22] C. Ge, X. Sang, W. Yao, L. Zhang, D. Wang, Unsymmetrical indazolyl-pyridinyl-triazole ligand-promoted highly active iridium complexes supported on hydrotalcite and its catalytic application in water, Green Chem. 20 (2018) 1805–1812, https://doi.org/10.1039/c7gc02892j.
[23] S. Hazra, A.K. Kushawaha, D. Yadav, P. Dolui, M. Deb, A.J. Elias, Table salt as a catalyst for the oxidation of aromatic alcohols and amines to acids and imines in aqueous medium: Effectively carrying out oxidation reactions in sea water, Green Chem. 21 (2019) 1929–1934, https://doi.org/10.1039/c9gc00497a.
[24] K. Wang, P. Jiang, M. Yang, P. Ma, J. Qin, X. Huang, L. Ma, R. Li, Metal-free nitrogen-doped carbon nanosheets: A catalyst for the direct synthesis of imines under mild conditions, Green Chem. 21 (2019) 2448–2461, https://doi.org/10.1039/c9gc00908f.
[25] C.P. Dong, A. Uematsu, S. Kumazawa, Y. Yamamoto, S. Kodama, A. Nomoto, M. Ueshima, A. Ogawa, 2,4,6-Trihydroxybenzoic Acid-Catalyzed Oxidative Ugi Reactions with Molecular Oxygen via Homo- And Cross-Coupling of Amines, J. Org. Chem. 84 (2019) 11562–11571, https://doi.org/10.1021/acs.joc.9b01422.
[26] C. Liu, N. Li, L. Peng, W. Zhong, L. Mao, D. Yin, Hydrothermal Carbonization of Renewable Natural Plants as Superior Metal-Free Catalysts for Aerobic Oxidative Coupling of Amines to Imines, ACS Sustainable Chem. Eng. 8 (2020) 11404–11412, https://doi.org/10.1021/acssuschemeng.0c03757.
[27] K. Das, A. Mondal, D. Srimani, Selective Synthesis of 2-Substituted and 1,2-Disubstituted Benzimidazoles Directly from Aromatic Diamines and Alcohols Catalyzed by Molecularly Defined Nonphosphine Manganese(I) Complex, J. Org. Chem. 83 (2018) 9553–9560, https://doi.org/10.1021/acs.joc.8b01316.
[28] P. Daw, Y. Ben-David, D. Milstein, Direct Synthesis of Benzimidazoles by Dehydrogenative Coupling of Aromatic Diamines and Alcohols Catalyzed by Cobalt, ACS Catal. 7 (2017) 7456–7460, https://doi.org/10.1021/acscatal.7b02777.
[29] S.P. Midya, J. Pitchaimani, V.G. Landge, V. Madhu, E. Balaraman, Direct access to: N -alkylated amines and imines via acceptorless dehydrogenative coupling catalyzed by a cobalt(II)-NNN pincer complex, Catal. Sci. Technol. 8 (2018) 3469–3473, https://doi.org/10.1039/c8cy00859k.
[30] A. Bakandritsos, R.G. Kadam, P. Kumar, G. Zoppellaro, M. Medved', J. Tuček, T. Montini, O. Tomanec, P. Andrýsková, B. Drahoš, R.S. Varma, M. Otyepka, M.B. Gawande, P. Fornasiero, R. Zbořil, Mixed-Valence Single-Atom Catalyst Derived from Functionalized Graphene, Adv. Mater. 31 (17) (2019) 1900323.
[31] X. Cui, W. Li, K. Junge, Z. Fei, M. Beller, P.J. Dyson, Selective Acceptorless Dehydrogenation of Primary Amines to Imines by Core-Shell Cobalt Nanoparticles, Angew. Chem. 132 (2020) 7571–7577, https://doi.org/10.1002/ange.201915526.
[32] T. Chutimasakul, P. Na Nakhonpanom, W. Tirdtrakool, A. Intanin, T. Bunchuay, R. Chantiwas, J. Tantirungrotechai, Uniform Cu/chitosan beads as a green and reusable catalyst for facile synthesis of iminesviaoxidative coupling reaction, RSC Adv. 10 (2020) 21009–21018, https://doi.org/10.1039/d0ra03884a.
[33] K. Junge, V. Papa, M. Beller, Cobalt-Pincer Complexes in Catalysis, Chem. Eur. J. 25 (2019) 122–143, https://doi.org/10.1002/chem.201803016.
[34] R. Shi, Z. Zhang, X. Hu, Nickamine and Analogous Nickel Pincer Catalysts for Cross-Coupling of Alkyl Halides and Hydrosilylation of Alkenes, Acc. Chem. Res. 52 (2019) 1471–1483, https://doi.org/10.1021/acs.accounts.9b00118.
[35] T.B. Nguyen, J. Le Bescont, L. Ermolenko, A. Al-Mourabit, Cobalt- and iron-catalyzed redox condensation of o-substituted nitrobenzenes with alkylamines: A step- and redox-economical synthesis of diazaheterocycles, Org. Lett. 15 (2013) 6218–6221, https://doi.org/10.1021/ol403064z.
[36] K. Gopalaiah, S.N. Chandrudu, Iron(II) bromide-catalyzed oxidative coupling of benzylamines with ortho-substituted anilines: Synthesis of 1,3-benzazoles, RSC Adv. 5 (2015) 5015–5023, https://doi.org/10.1039/c4ra12490a.
[37] E. Zhang, H. Tian, S. Xu, X. Yu, Q. Xu, Iron-catalyzed direct synthesis of imines from amines or alcohols and amines via aerobic oxidative reactions under air, Org. Lett. 15 (2013) 2704–2707, https://doi.org/10.1021/ol4010118.
[38] R.D. Patil, S. Adimurthy, Copper-Catalyzed Aerobic Oxidation of Amines to Imines under Neat Conditions with Low Catalyst Loading, Adv. Synth. Catal. 353 (2011) 1695–1700, https://doi.org/10.1002/adsc.201100100.
[39] K.M.H. Nguyen, M. Largeron, A Bioinspired Catalytic Aerobic Oxidative C-H Functionalization of Primary Aliphatic Amines: Synthesis of 1,2-Disubstituted Benzimidazoles, Chem. Eur. J. 21 (2015) 12606–12610, https://doi.org/10.1002/chem.201502487.
[40] M. Largeron, M.B. Fleury, A Bioinspired Organocatalytic Cascade for the Selective Oxidation of Amines under Air, Chem. Eur. J. 23 (2017) 6763–6767, https://doi.org/10.1002/chem.201701402.
[41] M. Largeron, M.-B. Fleury, A Biologically Inspired Cu(I)/Topaquinone-Like Co-Catalytic System for the Highly Atom-Economical Aerobic Oxidation of Primary Amines to Imines, Angew. Chem. 124 (2012) 5505–5508, https://doi.org/10.1002/ange.201200587.
[42] L.M. Kabadwal, S. Bera, D. Banerjee, Recent advances in sustainable organic transformations using methanol: Expanding the scope of hydrogen-borrowing catalysis, Org. Chem. Front. 8 (2021) 7077–7096, https://doi.org/10.1039/d1qo01412a.
[43] M. Rekha, A. Hamza, B.R. Venugopal, N. Nagaraju, Synthesis of 2-substituted benzimidazoles and 1,5-disubstituted benzodiazepines on alumina and zirconia catalysts, Cuihua Xuebao/Chinese, J. Catal. 33 (2012) 439–446, https://doi.org/10.1016/S1872-2067(11)60338-0.
[44] W.C. Lee, C.H. Wang, Y.H. Lin, W.C. Shih, T.G. Ong, Tandem isomerization and C-H activation: Regioselective hydroheteroarylation of allylarenes, Org. Lett. 15 (2013) 5358–5361, https://doi.org/10.1021/ol402644y.
[45] Y. Nakao, E. Morita, H. Idei, T. Hiyama, Dehydrogenative [4 + 2] cycloaddition of formamides with alkynes through double C-H activation, J. Am. Chem. Soc. 133 (2011) 3264–3267, https://doi.org/10.1021/ja1102037.
[46] H. Gao, L. Hu, Y. Hu, X. Lv, Y.B. Wu, G. Lu, Origins of Lewis acid acceleration in nickel-catalysed C-H, C-C and C-O bond cleavage, Catal, Sci. Technol. 11 (2021) 4417–4428, https://doi.org/10.1039/d1cy00660f.
[47] C. Wang, Z. Xi, Co-operative effect of Lewis acids with transition metals for organic synthesis, Chem. Soc. Rev. 36 (2007) 1395–1406, https://doi.org/10.1039/b608694m.
[48] B. Chatterjee, W.C. Chang, S. Jena, C. Werlé, Implementation of Cooperative Designs in Polarized Transition Metal Systems-Significance for Bond Activation and Catalysis, ACS Catal. 10 (2020) 14024–14055, https://doi.org/10.1021/acscatal.0c03794.
[49] Y. Deng, S. Kumar, H. Wang, Synergistic-cooperative combination of enamine catalysis with transition metal catalysis, Chem. Commun. 50 (2014) 4272–4284, https://doi.org/10.1039/c4cc00072b.
[50] E. Lopez, S.C. Thorp, R.S. Mohan, Bismuth(III) compounds as catalysts in organic synthesis: A mini review, Polyhedron. 222 (2022), https://doi.org/10.1016/j.poly.2022.115765 115765.
[51] M. Zahid, J. Li, A. Ismail, F. Zaera, Y. Zhu, Platinum and cobalt intermetallic nanoparticles confined within MIL-101(Cr) for enhanced selective hydrogenation of the carbonyl bond in a, ß-unsaturated aldehydes: synergistic effects of electronically modified Pt sites and Lewis acid sites, Catal. Sci. Technol. 11 (2021) 2433–2445, https://doi.org/10.1039/d0cy02082f.
[52] R. Mészáros, A. Márton, M. Szabados, G. Varga, Z. Kónya, Á. Kukovecz, F. Fülöp, I. Pálinkó, S.B. Ötvös, Exploiting a silver–bismuth hybrid material as heterogeneous noble metal catalyst for decarboxylations and decarboxylative deuterations of carboxylic acids under batch and continuous flow conditions, Green Chem. 23 (2021) 4685–4696, https://doi.org/10.1039/D1GC00924A.
[53] G. Varga, M. Kocsis, Á. Kukovecz, Z. Kónya, I. Djerdj, P. Sipos, I. Pálinkó, CuIBiOI is an efficient novel catalyst in Ullmann-type CN– couplings with wide scope—A rare non-photocatalytic application, Mol. Catal. 493 (2020), https://doi.org/10.1016/j.mcat.2020.111072 111072.
[54] M. Kocsis, S.B. Ötvös, G.F. Samu, Z. Fogarassy, B. Pécz, Á. Kukovecz, Z. Kónya, P. Sipos, I. Pálinkó, G. Varga, Copper-Loaded Layered Bismuth Subcarbonate—Efficient Multifunctional Heterogeneous Catalyst for Concerted C-S/C–N Heterocyclization, ACS Appl. Mater. Interfaces. 13 (2021) 42650–42661, https://doi.org/10.1021/acsami.1c09234.
[55] S.B. Ötvös, R. Mészáros, G. Varga, M. Kocsis, Z. Kónya, Á. Kukovecz, P. Pusztai, P. Sipos, I. Pálinkó, F. Fülöp, A mineralogically-inspired silver-bismuth hybrid material: An efficient heterogeneous catalyst for the direct synthesis of nitriles from terminal alkynes, Green Chem. 20 (2018) 1007–1019, https://doi.org/10.1039/c7gc02487h.

[56] R. Mészáros, S.B. Ötvös, G. Varga, É. Böszörményi, M. Kocsis, K. Karádi, Z. Kónya, Á. Kukovecz, I. Pálinkó, F. Fülöp, A mineralogically-inspired silver–bismuth hybrid material: Structure, stability and application for catalytic benzyl alcohol dehydrogenations under continuous flow conditions, Mol. Catal. 498 (2020) 111263.
[57] Y. Zhang, X. Zhang, Y. Ling, F. Li, A.M. Bond, J. Zhang, Controllable Synthesis of Few-Layer Bismuth Subcarbonate by Electrochemical Exfoliation for Enhanced CO_2 Reduction Performance, Angew. Chem. Int. Ed. 57 (2018) 13283–13287, https://doi.org/10.1002/anie.201807466.
[58] P. Wu, S. Dai, G. Chen, S. Zhao, Z. Xu, M. Fu, P. Chen, Q. Chen, X. Jin, Y. Qiu, S. Yang, D. Ye, Interfacial effects in hierarchically porous α-MnO_2/Mn_3O_4 heterostructures promote photocatalytic oxidation activity, Appl. Catal. B Environ. 268 (2020) 118418.
[59] L. Miao, X. Tang, S. Zhao, X. Xie, C. Du, T. Tang, H. Yi, Study on mechanism of low-temperature oxidation of n-hexanal catalysed by 2D ultrathin Co_3O_4 nanosheets, Nano Res. 15 (2022) 1660–1671, https://doi.org/10.1007/s12274-021-3746-8.
[60] P.F. Zhang, J.Y. Zhang, T. Sheng, Y.Q. Lu, Z.W. Yin, Y.Y. Li, X.X. Peng, Y. Zhou, J.T. Li, Y.J. Wu, J.X. Lin, B. Bin Xu, X.M. Qu, L. Huang, S.G. Sun, Synergetic Effect of Ru and NiO in the Electrocatalytic Decomposition of Li_2CO_3 to Enhance the Performance of a Li-CO_2/O_2 Battery, ACS Catal. 10 (2020) 1640–1651, https://doi.org/10.1021/acscatal.9b04138.
[61] R.J. Jia, J.T. Han, X.J. Wu, C.L. Wu, Y.H. Huang, W. Huang, Controllable synthesis and magnetic property of $BiMn_2O_5$ crystals, Mater. Res. Bull. 43 (2008) 1702–1708, https://doi.org/10.1016/j.materresbull.2007.07.023.
[62] M. Bernard, A. Hugot-Le Goff, B.V. Thi, S. Cordoba de Torresi, Electrochromic Reactions in Manganese Oxides: I. Raman Analysis, J. Electrochem. Soc. 140 (1993) 3065–3070. https://doi.org/10.1149/1.2220986.
[63] C. Murli, S.M. Sharma, S.K. Kulshreshtha, S.K. Sikka, High-pressure behavior of β-$Ni(OH)_2$ - A Raman scattering study, Phys. B Condens. Matter. 307 (2001) 111–116, https://doi.org/10.1016/S0921-4526(01)00646-9.
[64] B. Rivas-Murias, V. Salgueiriño, Thermodynamic CoO–Co_3O_4 crossover using Raman spectroscopy in magnetic octahedron-shaped nanocrystals, J. Raman Spectrosc. 48 (2017) 837–841, https://doi.org/10.1002/jrs.5129.
[65] J.L. Ortiz-Quiñonez, I. Zumeta-Dubé, D. Díaz, N. Nava-Etzana, E. Cruz-Zaragoza, P. Santiago-Jacinto, Bismuth Oxide Nanoparticles Partially Substituted with EuIII, MnIV, and SiIV: Structural, Spectroscopic, and Optical Findings, Inorg. Chem. 56 (2017) 3394–3403, https://doi.org/10.1021/acs.inorgchem.6b02923.
[66] H.Y. Xu, S. Le Xu, X.D. Li, H. Wang, H. Yan, Chemical bath deposition of hausmannite Mn_3O_4 thin films, Appl. Surf. Sci. 252 (2006) 4091–4096, https://doi.org/10.1016/j.apsusc.2005.06.011.
[67] J. Park, X. Shen, G. Wang, Solvothermal synthesis and gas-sensing performance of Co_3O_4 hollow nanospheres, Sensors Actuators, B Chem. 136 (2009) 494–498, https://doi.org/10.1016/j.snb.2008.11.041.
[68] M.K. Carpenter, D.A. Corrigan, Photoelectrochemistry of Nickel Hydroxide Thin Films, J. Electrochem. Soc. 136 (4) (1989) 1022–1026.
[69] Y. Yang, S. Wu, Y. Li, Q. Zhang, X. Zhao, Efficient UV-vis-IR photothermocatalytic selective ethanol oxidation on MnO:X/TiO_2 nanocomposites significantly enhanced by a novel photoactivation, J. Mater. Chem. A. 8 (2020) 1254–1264, https://doi.org/10.1039/c9ta12531k.
[70] M.G. Uytterhoeven, R.A. Schoonheydt, Diffuse reflectance spectroscopy of cobalt in wet and dry gels for probing the synthesis of CoAPO-5 and CoAPO-34, Microporous Mater. 3 (1994) 265–279, https://doi.org/10.1016/0927-6513(94)00041-7.
[71] H. Huang, X. Li, J. Wang, F. Dong, P.K. Chu, T. Zhang, Y. Zhang, Anionic Group Self-Doping as a Promising Strategy: Band-Gap Engineering and Multi-Functional Applications of High-Performance CO_3^{2-}-Doped $Bi_2O_2CO_3$, ACS Catal. 5 (2015) 4094–4103, https://doi.org/10.1021/acscatal.5b00444.
[72] M.C. Biesinger, B.P. Payne, A.P. Grosvenor, L.W.M. Lau, A.R. Gerson, R.S.C. Smart, Resolving surface chemical states in XPS analysis of first row transition metals, oxides and hydroxides: Cr, Mn, Fe, Co and Ni, Appl. Surf. Sci. 257 (2011) 2717–2730, https://doi.org/10.1016/j.apsusc.2010.10.051.
[73] M.C. Biesinger, B.P. Payne, L.W.M. Lau, A. Gerson, R.S.C. Smart, X-ray photoelectron spectroscopic chemical state quantification of mixed nickel metal, oxide and hydroxide systems, Surf. Interface Anal. 41 (2009) 324–332, https://doi.org/10.1002/sia.3026.
[74] A. Melli, S. Potenti, M. Melosso, S. Herbers, L. Spada, A. Gualandi, K.G. Lengsfeld, L. Dore, P. Buschmann, P.G. Cozzi, J.U. Grabow, V. Barone, C. Puzzarini, A Journey from Thermally Tunable Synthesis to Spectroscopy of Phenylmethanimine in Gas Phase and Solution, Chem. Eur. J. 26 (2020) 15016–15022, https://doi.org/10.1002/chem.202003270.